# Ultra-bright omni-directional collective emission of correlated photon pairs from atomic vapors

Y. P. Huang and M. G. Moore
*Department of Physics & Astronomy, Michigan State University, East Lansing, MI 48824*
(Dated: November 19, 2009)

Spontaneous four-wave mixing can generate highly correlated photon pairs from atomic vapors. We show that multi-photon pumping of dipole-forbidden transitions in a recoil-free geometry can result in ultra-bright pair-emission in the full $4\pi$ solid angle, while strongly suppresses background Rayleigh scattering and associated atomic heating, Such a system can produce photon pairs at rates of $\sim 10^{12}$ per second, given only moderate optical depths of $10 \sim 100$, or alternatively, the system can generate paired photons with sub-natural bandwidths at lower production rates. We derive a rate-equation based theory of the collective atomic population and coherence dynamics, and present numerical simulations for a toy model, as well as realistic model systems based on $^{133}$Cs and $^{171}$Yb level structures. Lastly, we demonstrate that dark-state adiabatic following (EIT) and/or timescale hierarchy protects the paired photons from reabsorption as they propagate through an optically thick sample.

PACS numbers: 42.65.Lm, 42.50.Ar, 42.50.Dv

## I. INTRODUCTION

The study of correlated/entangled photon pairs has long been a central topic in the field of quantum optics [1]. The importance of paired photons is two-fold: they i) provide powerful tools to test the peculiar aspects of quantum mechanics, such as violations of local-realism [2–4]; and ii) they hold promises for advancements in quantum measurement, communication, and information processing [5–11]. Over the past few decades, spontaneous parametric down-conversion (SPDC) in nonlinear crystals has been the standard source of photon pairs [12, 13]. More recently, an alternative class of biphoton sources has emerged, based on optical four-wave mixing (FWM) in atomic vapors [14–22]. These approaches rely on collective effects [23, 24] to greatly increase the probability of correlated emission events. Compared to SPDC, photon pairs generated via FWM in general have a much narrower bandwidth, significantly greater temporal and spatial coherence, and much higher conversion efficiencies. They are thus particularly suitable for hybrid quantum communications and computations employing atoms and photons [11, 25], and for high-precision quantum measurements and imaging [6, 10].

At present, FWM photon pair sources can be categorized into three types by level configuration. The first type, built on atomic two-level systems, is a connected double-Rayleigh emission process [26, 27]. Due to strong background Rayleigh scattering, however, the resulting pair correlation is very weak, without satisfying the necessary Cauchy criteria for biphoton correlation [18, 21]. A second type is configured on two-photon cascade emission in a four-level system [20, 28]. While high-fidelity photon pairs are generated, due to the unequal wavelengthes of two cascade photons, the phase-matching condition for collective emission can only be satisfied if the first photon is emitted by chance into a specific small solid-angle, thus unpaired emission dominates the overall radiation, resulting in a relatively low conversion efficiency. The third type employs Raman FWM (hereafter referred to as "RFWM") in multilevel systems, configured on double-$\Lambda$ [14, 17, 18, 21, 22] or "X" [19] level diagrams. The major challenge in these schemes is to suppress background Rayleigh scattering, which tends to rapidly overwhelm paired emission. Three approaches have been proposed to for this suppression, including i) using frequency selectors to filter out Rayleigh photons [17]; ii) collecting pairs along emission directions where the dipole pattern leads to zero Rayleigh emission [18]; and iii) using a single-mode optical cavity to suppress Rayleigh transitions [19]. While yielding up to $10^5$ pairs per second, all of these setups are unidirectional, where photon pairs are produced only along certain directions. This restricts the obtainable beam brightness of the photon pairs, since in each momentum mode, the time separation between pairs must be large relative to the correlation time. Lastly, in aforementioned FWM schemes where unpaired emissions dominate, atomic samples are rapidly thermalized due to random atomic recoils, limiting applications of these schemes to 'hot' vapors only.

Background Rayleigh scattering occurs when there is a spontaneous one-photon channel by which atoms can return to the initial internal hyperfine level without completing the desired biphoton emission cycle. We propose to eliminate this in RFWM by replacing the single pump laser with a multi-photon pump process that drives a one-photon dipole-forbidden transition. The second part of our proposal is to use 'recoil-free' pumping, meaning that the k-vectors of all of the driving fields sum to zero. Phase matching, which is enhanced by collective effects, will then be satisfied whenever the two paired photons have equal and opposite momenta, allowing paired emission into the full $4\pi$ solid angle. As a result, the biphoton emission rate will be enhanced by up to four orders of magnitude over unidirectional approaches. Furthermore, since Rayleigh scattering has been eliminated, atomic

thermalization will be strongly suppressed. Thus this scheme can also be applied in ultracold vapors including Bose-Einstein condensates (BECs), for which it might also be viewed as a novel in-situ non-demolition imaging technique.

A brief organization of this paper is as follows. In section II, we study a 'butterfly' biphoton protocol using a simplified model, which is a viable simplification of realistic configurations. In section III, we give two realistic implementations, one employing the 399nm-line transition in Ytterbium (section III A), and the other using the 852nm D2-line transition in Cesium (section III B). In section IV, we then address the critical issue of how to avoid reabsorption as the photon pairs propagate in an optically thick sample. This is followed by a discussion and conclusions in section V.

## II. BASIC MODEL

In this section, we will use a simplified 'toy model' to show the important physics of the butterfly scheme for ultra-bright photon-pairs. We present the schematic model in section II A, and employ a set of rate equations to solve for atomic dynamics in section II B. Then, we examine the time and polarization correlation of generated photon pairs in II C and II D. In section II E, we estimate the threshold temperature of the present biphoton source.

### A. Toy Level Scheme

A schematic level diagram of the butterfly scheme is shown in Fig. 1 (a). While greatly simplified with respect to a realistic level-scheme, this model will serve to illustrate the important dynamical effects. The physical mechanism is best illustrated in a quantum trajectory picture, as follows. A sample of atoms initially pumped into the $|1\rangle$ state, is first weakly coupled to the excited $|2\rangle$ level via a multi-photon pump process. This imparts a net recoil momentum of $\hbar\mathbf{K}$, so that for an initial momentum $\hbar\mathbf{q}$, an atom excited to $|2\rangle$ has a momentum of $\hbar(\mathbf{q}+\mathbf{K})$. This excited atom will then spontaneously decay to $|3\rangle$, emitting a 'signal' photon with a random momentum $\hbar\mathbf{k}$, shifting the atom's momentum to $\hbar(\mathbf{q}+\mathbf{K}-\mathbf{k})$. Decay from $|2\rangle$ back to state $|1\rangle$, which would generate background Rayleigh scattering, is forbidden by dipole selection-rules. The atom in state $|3\rangle$ is then rapidly repumped to $|4\rangle$ by a strong multi-photon coupling process. The coupling fields are arranged to yield a net momentum of $-\hbar\mathbf{K}$, leading to a momentum of $\hbar(\mathbf{q}-\mathbf{k})$ for the atom. From $|4\rangle$, the atom decays back to the $|1\rangle$ state, emitting an 'idler' photon. Collective effects will strongly enhance the scattering probability if the atom can be returned to its initial momentum state $\hbar\mathbf{q}$, which will result in the idler photon being emitted with momentum $-\hbar\mathbf{k}$.

The collective enhancement mechanism can be understood by noting first that the emission of the signal photon with momentum $\hbar\mathbf{k}$ imprints 'which atom' information onto the atomic ensemble via atomic recoil, provided of course that the single-photon recoil momentum is larger than the momentum coherence length of the sample (which for a thermal gas of free particles is the inverse sample length). If the idler photon is then emitted with phase-matched momentum, $\hbar\mathbf{k}_i = -\hbar\mathbf{k}$, then the atom is restored to its initial momentum state of $\hbar\mathbf{q}$, thus 'erasing' the 'which atom' information, so that many-body interference enhances the emission rate by a factor $N$. The 'which atom' information will be effectively erased only when the magnitude of the momentum difference between the initial and final states is less than or equal to the momentum coherence length of the atom, $|\mathbf{k}+\mathbf{k}_i| \lesssim k_{coh}$, which leads to a collective emission solid-angle of $\Omega_{coh} \sim \pi(k_{coh}/k)^2$. For a lone atom, and neglecting the dipole emission pattern, the probability of correlated emission, i.e. the probability of $\mathbf{k}_i$ falling within $\Omega_{coh}$ of $-\mathbf{k}$, is $P_c(1) = \Omega_{coh}/4\pi$ with a non-correlated probability $P_{nc}(1) = 1 - \Omega_{coh}/4\pi$. For a sample of $N$ atoms, the differential probability inside $\Omega_{coh}$ is enhanced by $N$ relative to the differential probability outside $\Omega_{coh}$, leading to a collectively enhanced correlated emission probability of $P_c(N) = N\Omega_{coh}/(N\Omega_{coh}+4\pi-\Omega_{coh})$. The probability of non-correlated emission is correspondingly reduced by unitarity to $P_{nc}(N) = (4\pi-\Omega_{coh})/(N\Omega_{coh}+4\pi-\Omega_{coh})$. Under the condition $N\Omega_{coh}/4\pi \gg 1$, the probabilities are then given approximately by $P_c(N) = 1-4\pi/N\Omega_{coh} \sim 1$ and $P_{nc}(N) \approx 4\pi/N\Omega_{coh} \ll 1$. For a thermal sample of dimension $L$, we have $k_{coh} \sim 1/L$, so that $\Omega_{coh} \sim \pi/(kL)^2$. This gives a correlated emission probability of $P_c = 1-1/D$, where $D = N/(2kL)^2 = n\lambda^2 L/16\pi^2$ is the optical depth of the sample. Other considerations aside, we clearly see that strong photon pair-correlations in $k$-space are achieved by maximizing the optical thickness of the sample.

The fact that the driving and coupling fields have zero net momenta makes the scheme in a limited sense 'recoil-free', so that phase-matched collective emission can occur regardless of which direction the signal photon randomly 'chooses'. This is illustrated in Fig. 1 (b), where for an arbitrarily chosen $\mathbf{k}$, the atomic dynamics in the space of recoil momentum undergoes a closed, diamond-like cycle. This distinguishes the present setup from competing biphoton protocols employing non-counter-propagating driving and coupling, where pair emissions are restricted to be in a plane perpendicular to the nonzero net momentum [17, 18, 20, 28].

### B. Population Dynamics

To study the system's dynamics, we quantize the atomic center-of-mass motion, onto the eigenmodes, $\{|\mathbf{q}\rangle\}$, of a box of dimension $L$, where $L$ is the ensemble dimension. As the box traverse time, $L/v$, is long com-

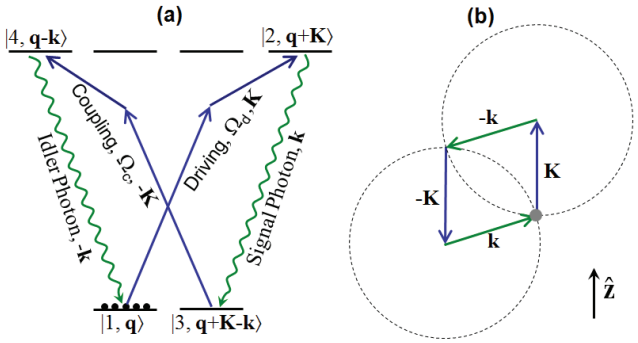


FIG. 1: (Color online) A schematic model of the butterfly scheme. Figure (a) draws the simplified level diagram, employing multi-photon driving and coupling pumps. The notation $|j, \mathbf{k}\rangle$ indicates a single atom state in internal level $|j\rangle$ and with momentum $\hbar\mathbf{k}$. The momentum $\hbar\mathbf{K}$ is the net momentum of the multiphoton transition from levels $|1\rangle$ to $|2\rangle$. Figure (b) shows how a phase-matched diamond-like cycle in atom-recoil momentum space exists for any signal photon emission direction.

pared to the relevant dynamic timescale, $(\Gamma)^{-1}$, we can safely impose periodic boundary conditions, so that the allowed $\mathbf{q}$ values lie on a three-dimensional cubic lattice with spacing $2\pi/L$. Eliminating the scattered light-field via the Markoff approximation, and taking into account the exchange-type symmetry respected by the Hamiltonian and the initial conditions, allows us to derive a set of rate equations for the atomic population dynamics. The advantage of rate equations, as opposed to a mean-field approach, is that spontaneous decay is incorporated via the usual $(N+1)$ factors, thus avoiding the need for noise operators. For the toy model depicted in Fig. 1 (a), the rate equations are:

$$\frac{d}{dt}N_1 = \frac{i}{2}\left(\Omega_d\varrho_{21} - c.c\right) + \sum_{\mathbf{q}}\Gamma_4\beta_{\mathbf{q}4}N_{\mathbf{q}4}(N_1+1), \quad (1)$$

$$\frac{d}{dt}N_2 = -\frac{i}{2}\left(\Omega_d\varrho_{21} - c.c\right) - \sum_{\mathbf{q}}\Gamma_2\beta_{\mathbf{q}2}N_2(N_{\mathbf{q}3}+1), \quad (2)$$

$$\frac{d}{dt}\varrho_{21} = i\frac{\Omega_d}{2}(N_1 - N_2) + \frac{1}{2}\varrho_{21}\sum_{\mathbf{q}}\left[\Gamma_4\beta_{\mathbf{q}4}N_{\mathbf{q}4} - \Gamma_2\beta_{\mathbf{q}2}(N_{\mathbf{q}3}+1)\right], \quad (3)$$

$$\frac{d}{dt}N_{\mathbf{q}3} = \frac{i}{2}\left(\Omega_c\varrho_{\mathbf{q}43} - c.c\right) + \Gamma_2\beta_{\mathbf{q}2}N_2(N_{\mathbf{q}3}+1), \quad (4)$$

$$\frac{d}{dt}N_{\mathbf{q}4} = -\frac{i}{2}\left(\Omega_c\varrho_{\mathbf{q}43} - c.c\right) - \Gamma_4\beta_{\mathbf{q}4}N_{\mathbf{q}4}(N_1+1), - \Gamma_4(1-\beta_{\mathbf{q}4})N_{\mathbf{q}4} \quad (5)$$

$$\frac{d}{dt}\varrho_{\mathbf{q}43} = i\frac{\Omega_c}{2}(N_{\mathbf{q}3} - N_{\mathbf{q}4}) + \frac{1}{2}\varrho_{\mathbf{q}43}\times \left[\Gamma_2\beta_{\mathbf{q}2}N_2 - \Gamma_4\beta_{\mathbf{q}4}(N_1+1) - \Gamma_4(1-\beta_{\mathbf{q}4})\right], \quad (6)$$

a detailed derivation of these equations, as well as precise definitions of the variables, is presented in appendix A. Oversimplifying slighty, we can think of $N_1$ and $N_2$ as the populations of state $|1\rangle$ and $|2\rangle$, respectively, with $\varrho_{21}$ being the corresponding coherence operator. $N_{\mathbf{q}3}$ is the expectation number of atoms collectively excited into state $|3\rangle$ via emission of a signal photon with $\mathbf{k} \approx -\mathbf{q}$. Similarly, $N_{\mathbf{q}4}$ is the expectation number of these atoms transferred to state $|4\rangle$ by the coupling laser, while $\varrho_{\mathbf{q}43}$ is the coherence between these two collective states. Lastly, $\Omega_d$ and $\Omega_c$ are the effective Rabi frequencies of the driving and coupling transitions. The spontaneous emission rates for $|2\rangle \rightarrow |3\rangle$ and $|4\rangle \rightarrow |1\rangle$ decays, are $\Gamma_2$ and $\Gamma_4$, respectively, and $\beta_{\mathbf{q}2}$ and $\beta_{\mathbf{q}4}$ are the branching ratios for emission into the coherent-emission solid angle $\Omega_{coh} = \pi/(kL)^2$, with respect to the $\pm\mathbf{q}$ directions. For a spherical sample of radius $L/2$, a careful calculation [29] gives

$$\beta_{\mathbf{q}\mu} = (1 - |\hat{q}\cdot\hat{d}_\mu|^2)\frac{3}{8\pi}\left(\frac{\lambda}{L}\right)^2; \quad \mu = 2,4; \quad (7)$$

where $\hat{d}_2$, and $\hat{d}_4$ are the unit vectors along the dipole moments of the $|2\rangle \rightarrow |3\rangle$ and $|4\rangle \rightarrow |1\rangle$ transitions. Aside from dipole-emission factor, $(1 - |\hat{q}\cdot\hat{d}_j|^2)$, this is in good agreement of our initial estimate $\Omega_c/4\pi \sim \lambda^2/(4\pi L)^2$. The quantity $D_{\mathbf{q}4} = N_1\beta_{\mathbf{q}4}$ is then the optical depth along the $\pm\mathbf{q}$ directions, with respect to the $|1\rangle \leftrightarrow |4\rangle$ transition.

Strictly speaking, in the toy model, atoms which spontaneously decay from $|4\rangle$ to $|1\rangle$ by emitting rogue photons can still participate in the next-round pair-emission cycle, as the initial momentum of the atoms in state $|1\rangle$ is irrelevant to the collectivity (in the Doppler-free regime). This recycling process can be included in the rate-equation model by inserting a re-feeding term $\sum_{\mathbf{q}}\Gamma_4(1-\beta_{\mathbf{q}4})N_{\mathbf{q}4}$ to equation (1). In this case, the total atom number $N_1 + N_2 + \sum_{\mathbf{q}}N_{\mathbf{q}3} + N_{\mathbf{q}4}$ will be conserved, while still correctly describing the emission of rogue (uncorrelated) photons. In realistic schemes, however, atoms can also spontaneously decay to other ground levels which are not shown in figure 1, and/or they can decay from intermediate pumping levels to $|3\rangle$. These atoms will not be able to participate in further collective emission cycles, unless the are somehow repumped back to $|1\rangle$. Thus to avoid overly optimistic predictions, we have chosen not include the recycling process in the rate-equation model. It is noted that by completely excluding the recycling process, the pair generation rate is *underestimated*, as a fraction of rogue-photon emitting atoms will always be recycled. On the other hand, atoms which decay from $|4\rangle$ into levels other than $|1\rangle$ may be repeatedly re-excited to other levels by the pumping fields, and thus emit additional rogue photons. If such rogue photons can not be filtered out, they will contribute to the impurity of the collected biphoton beams. For present, however, we only focus on the short-time behavior of the system, up to a point when the atom loss is about 10%. In this time interval, the present dynamical model with rate equations (1)-(6) is reasonably valid.

The total emission rates for signal and idler photons, corresponding to the (enhanced) decay rates of the $|2\rangle$ and $|4\rangle$ levels, are

$$R_S = \Gamma_2 \sum_{\mathbf{q}} \beta_{\mathbf{q}2} N_2 (N_{\mathbf{q}3} + 1), \quad (8)$$

$$R_I = \Gamma_4 \sum_{\mathbf{q}} \beta_{\mathbf{q}4} N_{\mathbf{q}4} (N_1 + 1), \quad (9)$$

respectively. Assuming steady-state, clearly we must have $R_I \leq R_S$. If $R_I < R_S$, more signal photons are generated than idler photons, so that pairing is weak. Thus, at a minimum, strong pairing requires $R_I = R_S$. Focusing on a single $\mathbf{q}$ mode, and assuming $\beta_{\mathbf{q}2} = \beta_{\mathbf{q}4}$ and $\Gamma_2 = \Gamma_4$, we find

$$\frac{R_I(\hat{k})}{R_S(\hat{k})} = \left(\frac{N_1 + 1}{N_2}\right)\left(\frac{N_{\mathbf{q}4}}{N_{\mathbf{q}3} + 1}\right). \quad (10)$$

If we assume a strong drive, $\Omega_d \gtrsim \Gamma_2$, we have $N_2 \sim N_1$, which means we must also have $N_{\mathbf{q}4} \sim N_{\mathbf{q}3} \gg 1$, which in turn requires a strong coupling field, $\Omega_c \gtrsim \Gamma_4 \beta_{\mathbf{q}4} N_1$. We find, however, that dynamically this approach doesn't work, as it leads to a build-up of population in $N_{\mathbf{q}3}$ and $N_{\mathbf{q}4}$ without strong pairing. This leaves the case of weak driving, $\Omega_d \ll \Gamma_2$ so that $N_2 \ll N_1$. This then requires $N_{\mathbf{q}4} = \frac{N_2(N_{\mathbf{q}3}+1)}{N_1}$, which can be arranged by adjusting the drive and coupler strengths and detunings, and provided $N_{\mathbf{q}4} \ll 1$, results in strong pairing [18, 22].

The impurity of collected biphoton beams in the present toy-model comes from spontaneous emission of rogue idler photons into non phase-matched angles. The total emission rate of rogue photon is given by $R_{rogue} = \Gamma_4 \sum_{\mathbf{q}} N_{\mathbf{q}4}(1 - \beta_{\mathbf{q}4}) \approx \Gamma_4 \sum_{\mathbf{q}} N_{\mathbf{q}4}$, where $\beta_{\mathbf{q}4} \ll 1$. The ratio of paired idler to rogue idler photons is then given by $R_I/R_{rogue} = (N_1 + 1)\bar{\beta}$, where $\bar{\beta} = \sum_{\mathbf{q}} \beta_{\mathbf{q}4} N_{\mathbf{q}4} / \sum_{\mathbf{q}} N_{\mathbf{q}4}$ is the mean collectivity averaging over emission angles. For a spherical cloud of radius $R$, this is roughly $\lambda^2/16\pi R^2$. Defining the optical depth of a spherical cloud as $D = N_1\bar{\beta}$, the pair to rogue ratio is simply $R_I/R_{rogue} = D$, i.e., the optical depth. For typical samples of $D \sim 100$, there is then about one rogue photon per 100 pairs.

In general, the emission of a rogue photon leads to heating of the sample, due to random non-zero net-recoil. In a unidirectional scheme, the vast majority of photons are not paired, so that heating occurs at the usual single-photon decay spontaneous heating rate. Such schemes are thus only applicable to samples well above the recoil temperature. With the omnidirectional approach, the majority of spontaneous photons come in correlated pairs and thus impart no recoil kick. The heating rate is then reduced by a factor of the optical depth $D$, which should allow interesting experiments to be performed at or below the recoil temperature. For example, if a BEC of $N$ atoms is used as an omnidirectional biphoton source, the condensate only depletes at a rate of $R_{rogue}$, so that, e.g. $ND/10 \approx 10N$ photon pairs could be generated with only 10% of the condensate atoms being lost. This means that if desired, the present butterfly scheme can be used to directly image condensates *in situ*, in a relatively nondestructive manner. In other words, the BEC would exhibit resonance fluorescence, but with strongly suppressed heating. The additional brightness might, e.g., yield improved atom-number estimation.

Similarly to the case of two-photon cascade emission [2], here the bandwidth of both signal and idler photons in the strong coupling regime ($|\Omega_c| \gg D\Gamma_4$) is given by $\Gamma_4 D/2$, where $\Gamma_4 D$ is the superradiance broadened linewidth of state $|4\rangle$. This is because the intermediate $|3\rangle$ and $|4\rangle$ levels participate the pair emission by first forming dressed states of $|\pm\rangle = (|3\rangle \pm |4\rangle)/\sqrt{2}$. The process of pair emission depicted in figure 1 is then physically equivalent to cascade emission from $|2\rangle$ to $|1\rangle$, through either $|+\rangle$ or $|-\rangle$ states. In further analogy to cascade emission, the frequency-sum of the signal and idler photons has a much narrower linewidth of $|\Omega_d|^2/\Gamma_2$, as given by the reciprocal of the pair emission time. In the weak coupling regime, $|\Omega_c| \ll D\Gamma_4$, the coupling dynamics is overdamped, so that the $|4\rangle$ level can be adiabatically eliminated. Then the pair emission is effectively through the $|3\rangle$ level only, the linewidth of which is broadened from zero to $|\Omega_c|^2/D\Gamma_4$ by the coupling laser. This, together with the fact that we choose $|\Omega_c|^2/D\Gamma_4 \gg |\Omega_d|^2/\Gamma_2$ for a strong pairing effect, gives a bandwidth of $\frac{|\Omega_c|^2}{D\Gamma_4} \ll D\Gamma_4$ for the emitted photons. In the very weak coupling limit, with $|\Omega_c| < \sqrt{D}\Gamma_4$, this means that correlated photon pairs of sub-natural bandwidth can be generated.

To study the performance of this system, we numerically solve equations (1)-(6). One question that must be decided is how-many and which box eigenmodes need to be included in the simulation. Firstly, we note that in momentum space, the width of the energy shell for the signal photons is $\Delta k = \Gamma_4 D/c \sim 1\text{m}^{-1}$, while the size of a single eigenmode is $1/L$. Thus for normal sample sizes of $L \ll 1$m, only a single shell of modes of radius $2\pi/\lambda$ participates in the dynamics, where $\lambda \sim 10^{-7}$m is the wavelength of the $|2\rangle \rightarrow |3\rangle$ transition. This leads to a mode number of $M = 4\pi/\Omega_c \sim (L/\lambda)^2$, which could range anywhere from $10^4$ to $10^{10}$, depending on the sample size. To handle the dipole pattern, we then sort these modes $\{\mathbf{q}\}$ into 15 groups. The $j$-th ($j = 1, 2, ...15$) group contains those quasi-modes satisfying $\theta_{\mathbf{q}} \in [\theta_j, \theta_j + \pi/30)$, where $\theta_j = (j-1)\pi/30$, and $\theta_{\mathbf{q}} \in (0, \pi/2]$ is the angle between $\mathbf{q}$ and the $\hat{d}_2$ axis. Modes in the $j^{th}$ group, are assigned with mean collectivity parameters, $f_{j2}$, and $f_{j4}$, obtained by averaging over modes inside the group. In this approximation, all quasi modes within the same group will yield identical dynamics, so that only of one mode in each group needs to be included in the dynamical model. The effects of the other modes can then be included by weighting each representative mode by the number of modes on the interval $[\theta_j - \pi/30, \theta_j) \sim (L/\lambda)^2 \sin(j\pi/30)$. In this way, we are able to reduce the number of coupled rate equations from $10^4$-$10^{10}$, down to fewer than 100, while still incorporating the effects of the dipole radiation pat-

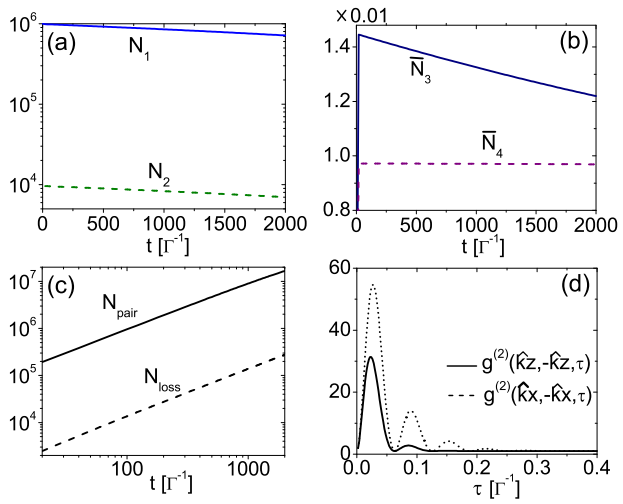


FIG. 2: (Color online) Figures (a)-(b) show the evolutions of $N_1, N_2, \overline{N}_3, \overline{N}_4$, while (c) compares the number of generated photon pairs $N_{pair}$ and lost atoms $N_{loss}$. Figure (d) plots the second-order correlation function $g^{(2)}(\mathbf{k}, -\mathbf{k}, \tau)$ for $\mathbf{k} = k\hat{z}$ and $\mathbf{k} = k\hat{x}$, respectively. Parameters are given in text.

tern.

We consider an example of $N = 10^6$ atom, with a spherically-symmetric Gaussian density distribution of radius $L = 34\lambda$, corresponding to an optical depth of $D = 70$. We consider resonant driving and coupling pumps propagating along $\hat{z}$ and $-\hat{z}$ directions, and take $\Gamma_2 = \Gamma_4 \equiv \Gamma$, $\Omega_d = 0.1\Gamma$, and $\Omega_c = 100\Gamma$. The results are shown in Fig. 2 (a)-(d). In figure (a), we plot the time evolution of $N_1, N_2$, showing that at all times only a small fraction of atoms are excited, i.e. $N_2 \ll N_1$, as required. In figure (b), we plot the mean atomic collective excitation numbers $\overline{N}_3$ and $\overline{N}_4$, obtained by averaging over $\mathbf{q}$. Both are found to be of order of 0.01, so that there is negligible overlap between subsequent pairs in a given mode. The total photon-pair number and lost atom number are shown in figure (c), where they are found to increase linearly in time with fitted rates of $8.3 \times 10^3\Gamma$ and $1.4 \times 10^2\Gamma$.

### C. Photon Pair Correlation

To estimate the time correlation of the two photons, we calculate the time-averaged second-order correlation function $g^{(2)}(\mathbf{k}, -\mathbf{k}, \tau)$, defined as [2]

$$g^{(2)}(\mathbf{k}, -\mathbf{k}, \tau) = \frac{1}{T}\int_0^T dt \times \frac{\langle \hat{a}^\dagger_{\mathbf{k}s}(t)\hat{a}^\dagger_{-\mathbf{k}i}(t+\tau)\hat{a}_{-\mathbf{k}i}(t+\tau)\hat{a}_{\mathbf{k}s}(t)\rangle}{\langle \hat{a}^\dagger_{\mathbf{k}s}(t)\hat{a}_{\mathbf{k}s}(t)\rangle\langle \hat{a}^\dagger_{-\mathbf{k}i}(t+\tau)\hat{a}_{-\mathbf{k}i}(t+\tau)\rangle}, \quad (11)$$

where $\hat{a}_{\mathbf{k}s}$ and $\hat{a}_{\mathbf{k}i}$ are the annihilation operators for signal and idler photons, which may or may not differ in polarization for a given $\mathbf{k}$, and $T$ is the averaging window. The correlation function is evaluated by first using adiabatic following to write the photon operators in terms of the atomic operators, where

$$\hat{a}_{\mathbf{k}s}(t) = \hat{a}_{\mathbf{k}s}(0)e^{-i\omega_{\mathbf{k}}t} - ig_{\mathbf{k}}\frac{\sin[(\omega_s-\omega_{\mathbf{k}})t/2]}{(\omega_s-\omega_{\mathbf{k}})t/2} \times e^{-i(\omega_s+\omega_{\mathbf{k}})t/2}\hat{\sigma}_{2,\mathbf{k}3}, \quad (12)$$

$$\hat{a}_{\mathbf{k}i}(t) = \hat{a}_{\mathbf{k}i}(0)e^{-i\omega_{\mathbf{k}}t} - ig_{\mathbf{k}}\frac{\sin[(\omega_s-\omega_{\mathbf{k}})t/2]}{(\omega_s-\omega_{\mathbf{k}})t/2} \times e^{-i(\omega_s+\omega_{\mathbf{k}})t/2}\hat{\sigma}_{\mathbf{k}4,1}. \quad (13)$$

Here, $g_{\mathbf{k}}$ is the atom-photon coupling constant, $\omega_{\mathbf{k}} = c|\mathbf{k}|$ is the photon's frequency, and $\omega_s$ is the resonance transition frequency. The collective atomic operators are defined as

$$\hat{\sigma}_{2,\mathbf{k}3} = \hat{\sigma}^\dagger_{\mathbf{k}3,2} = \sum_{\mathbf{q},\mathbf{Q}} f(\mathbf{k}+\mathbf{q}-\mathbf{Q})\hat{S}_{\mathbf{Q}2\mathbf{q}3} \quad (14)$$

$$\hat{\sigma}_{\mathbf{k}4,1} = \hat{\sigma}^\dagger_{1,\mathbf{k}4} = \sum_{\mathbf{q},\mathbf{Q}} f(\mathbf{k}+\mathbf{q}-\mathbf{Q})\hat{S}_{\mathbf{Q}4\mathbf{q}1} \quad (15)$$

where the ensemble operator $\hat{S}_{\mu\nu}$ and the structure function $f(\mathbf{k}+\mathbf{q}-\mathbf{Q})$ for the atomic sample are precisely defined in appendix A, Eq. (A18) and (A20), respectively. Inserting this result to the correlation function (11) gives

$$g^{(2)}(\mathbf{k}, -\mathbf{k}, \tau) = \frac{1}{T}\int_0^T dt \times \frac{\langle \hat{\sigma}_{\mathbf{k}3,2}(t)\hat{\sigma}_{1,\mathbf{k}4}(t+\tau)\hat{\sigma}_{\mathbf{k}4,1}(t+\tau)\hat{\sigma}_{2,\mathbf{k}3}(t)\rangle}{\langle \hat{\sigma}_{\mathbf{k}3,2}(t)\hat{\sigma}_{2,\mathbf{k}3}(t)\rangle\langle \hat{\sigma}_{1,\mathbf{k}4}(t+\tau)\hat{\sigma}_{\mathbf{k}4,1}(t+\tau)\rangle}, \quad (16)$$

where any contribution from vacuum electromagnetic (EM) fluctuations, given by $\hat{a}_{\mathbf{k}s}(0)$ and $\hat{a}_{\mathbf{k}s}(0)$, vanishes when tracing over the EM vacuum.

As demonstrated in detail in Appendix A, because our system is in a symmetric collective state throughout the dynamics, the products of coherence operators can be written as the products of number operators. Applying this to equation (16), we have

$$g^{(2)} \approx \frac{1}{T}\int_0^T dt \frac{\langle \hat{\sigma}_{\mathbf{q}3,2}(t)\hat{N}_{\mathbf{q}4}(t+\tau)\hat{\sigma}_{2,\mathbf{q}3}(t)\rangle}{N_{\mathbf{q}4}(t+\tau)N_2(t)(N_{\mathbf{q}3}(t)+1)}, \quad (17)$$

where we have replaced the number operator $\hat{N}_1$ with its meanfield $N_1$ and approximated $N_1+1 \approx N_1$. This result is a valid approximation as the $|1\rangle$ level is macroscopically occupied, with $N_1 \gg 1$. The discrete momentum $\mathbf{q}$ is the nearest neighbor of $\mathbf{k}$, with which $|\mathbf{k}-\mathbf{q}|$ is minimized.

Following the standard procedure [2], we write

$$N_{\mathbf{q}4}(t+\tau) = \sum_{j=1}^{2}\chi_j(\tau)N_j(t) + \sum_{j=3}^{4}\chi_j(\tau)N_{\mathbf{q}j}(t) + [\eta_1(\tau)\varrho_{12}(t) + \eta_2(\tau)\varrho_{\mathbf{q}34}(t) + c.c], \quad (18)$$

where we have used the fact that the coherent terms $\langle\hat{\varrho}_{\mathbf{q}32}\rangle$ and $\langle\hat{\varrho}_{\mathbf{q}41}\rangle$ are zero throughout the dynamics, since neither pumping nor purely spontaneous/superradiant decay processes will generate such coherences. The coefficients $\chi_j(\tau)$ and $\eta_j(\tau)$ are determined by studying the linear response of $N_{\mathbf{q}4}(t+\tau)$ to small perturbations in each variable, via numerically solving the rate equations (1)-(6). For instance, to determine $\chi_3(\tau)$, we apply a small, instant perturbation $\delta N_{\mathbf{q}3}$ to the system dynamics, i.e., making $N_{\mathbf{q}3}(t) \to N_{\mathbf{q}3}(t)+\delta N_{\mathbf{q}3}$. We then calculate the resulting drift $\delta N_{\mathbf{q}4}(t+\tau)$ from the unperturbed value $N_{\mathbf{q}4}(t+\tau)$, with which the coefficient is determined as $\chi_3(\tau) = \frac{\delta N_{\mathbf{q}4}(t+\tau)}{\delta N_{\mathbf{q}3}(t)}$.

Following the quantum regression theorem [30], in equation (17) we write $\hat{N}_{\mathbf{q}4}(t+\tau)$ at time $t+\tau$ in terms of operators at time $t$, using the result (18). The resulting expression is then normalized and factorized into products of the occupation numbers, giving

$$g^{(2)} = 1 + \frac{1}{T}\int_0^T dt \left( \frac{\chi_3(\tau)-\chi_2(\tau)}{N_{\mathbf{q}4}(t+\tau)} + \frac{\eta_1^*(\tau)\varrho_{12}(t)}{N_2(t)N_{\mathbf{q}4}(t+\tau)} + \frac{\eta_2^*(\tau)\varrho_{\mathbf{q}43}(t)}{(N_{\mathbf{q}3}(t)+1)N_{\mathbf{q}4}(t+\tau)} \right). \quad (19)$$

As seen in figure 2 (a) and (b), the atomic dynamics undergoes quasi-steady-state evolution, with slow damping due to atom losses. This allows us to approximate the populations and coherences as constants for the time period of interests, while effectively taking $T \to \infty$.

As seen in equation (19), a strong time correlation between signal and idler photons requires $N_{\mathbf{q}4} \ll 1$. Physically, this is because the one-to-one correspondence between signal and idler photons will be spoiled if there is more than one 'atom' in the same collective mode at the same time. This result agrees with the established experimental criteria, where the driving field must be weak such that most atoms remain in the initial ground state [17, 18]. In this weak driving regime, we find to a good approximation that

$$g^{(2)} \approx 1 + \frac{1}{< N_{\mathbf{q}4} >}\chi_3(\tau), \quad (20)$$

with $< N_{\mathbf{q}4} >$ being the time-averaging value of $N_{\mathbf{q}4}$.

For a weak coupling between $|3\rangle$ and $|4\rangle$ with $\Omega_c \ll D\Gamma_4$, we find $\chi_3(\tau) \approx \frac{|\Omega_c|^2}{D^2\Gamma_4^2} \ll 1$, which leads a time delay $\frac{D\Gamma_4}{|\Omega_c|^2}$ between signal and idler photons. A strong signal-idler correlation with $g^{(2)} \gg 1$ then requires $N_{\mathbf{q}4}$ to be very small. Since the pair generation rate $R_I \sim N_{\mathbf{q}4}$, this would ultimately limit the achievable beam brightness of photon pairs. For a strong coupling with $\Omega_c \gtrsim D\Gamma_4$, however, we find $\chi_3(\tau) \approx \sin^2\left(\frac{1}{2}\Omega_c\tau\right)\exp(-\frac{1}{2}D\Gamma_4\tau) \sim 1$. In this case, a relatively larger $N_{\mathbf{q}4}$ can give the same correlation, thus elevating the obtainable beam brightness. The correlation function in this case exhibits oscillatory and damped behaviors with sharp peaks, associated with Rabi-oscillations between $|3\rangle \leftrightarrow |4\rangle$ [17]. The time delay between signal and idler photons is roughly $(D\,\Gamma_4)^{-1}$. We note in all regimes, the bandwidth of signal and idler photons is the reciprocal of the delay time. In figure 2 (d), we plot the second-order correlation functions for photon pairs propagating along $\pm\hat{z}$ and $\pm\hat{x}$ directions. Both cases exhibit sharp peaks of widths $\sim 0.05\Gamma^{-1}$, indicating strong temporal correlation which violates the standard Cauchy-Schwartz inequality by a factor $\gtrsim 1000$.

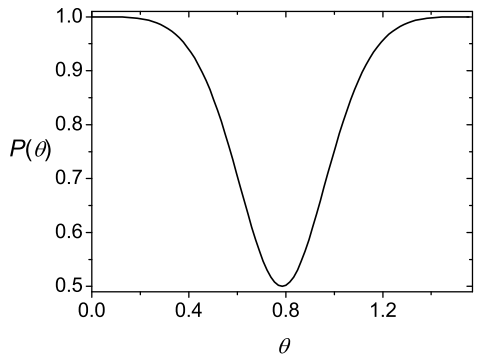


FIG. 3: The probability $P(\theta)$ for paired photons to be in opposite polarizations as a function of emission angle $\theta$, calculated for the toy model.

### D. Polarization entanglement

We now examine the polarization entanglement of paired photons. We consider a pair of signal and idler photon individually travelling along $\hat{k}$ and $-\hat{k}$ directions, with $\hat{k}(\theta,\phi) = \sin\theta\cos\phi\hat{x} + \sin\theta\cos\phi\hat{y} + \cos\theta\hat{z}$, where $\hat{z}$ is along the $\mathbf{K}$ direction. For $\hat{d}_{2,4} = \frac{1}{\sqrt{2}}(\hat{x} \pm i\hat{y})$, the probabilities for signal photons to be left and right circularly polarized along $\mathbf{k}$, denoted as $\hat{\epsilon}_L$ and $\hat{\epsilon}_R$, are $\beta_S^L(\theta) = \left(1+\cot^4\frac{\theta}{2}\right)^{-1}$ and $\beta_S^R(\theta) = \beta_S^L(\pi-\theta)$, respectively. Similarly, for the idler photons we have $\beta_I^R = \beta_S^L(\theta)$, and $\beta_I^L = \beta_S^R(\theta)$. The probability for photons to be in opposite circular polarizations along $\mathbf{k}$ (thus in the same polarizations along each's propagating direction) is then

$$P(\theta) = \beta_s^L(\theta)\beta_I^R(\theta) + \beta_s^R(\theta)\beta_I^L(\theta) = \frac{1+\cot^8\frac{\theta}{2}}{\left(1+\cot^4\frac{\theta}{2}\right)^2}. \quad (21)$$

As seen in Fig. 3, this is extremely flat around $\theta = 0, \pi$, where $P(\theta) \approx 1 - \frac{1}{8}\mathrm{mod}(\theta,\pi)^4 \approx 1$, meaning that photon pairs emitted over a wide range of $\theta$ will yield strong polarization entanglement. Due to the temporal overlap of signal and idler photons, each pair emitted within the strong correlation angle is approximately in the Bell state of $|\Psi^+\rangle = \frac{1}{\sqrt{2}}(|\epsilon_R\epsilon_L\rangle + |\epsilon_L\epsilon_R\rangle)$. For example, pairs with one photon emitted within $\theta < 0.5$ (corresponding to 17% of total emitted pairs) have an entanglement fidelity $\geq 99\%$.

### E. Critical Temperature

A biphoton source in an atomic ensemble relies on collective enhancement (superradiance) to increase the probability of correlation emission events, i.e. enforce 'phase matching' for the light waves. A necessary condition for collectivity is that the Doppler linewidth is smaller than the photon's superradiance-broadened linewidth, the latter of which is a factor $D$ greater than the natural linewidth [31, 32]. Physically, this condition is required to suppress dephasing of the collective atomic excitation during the superradiant emission process. The present scheme is recoil-free in the sense that the driving and coupling fields have net zero momenta, so that phase matching requires only that the signal and idler photons have equal and opposite momenta. However, an atom undergoing the biphoton emission cycle does possess a nonzero recoil momentum while in the intermediate states $|2\rangle$, $|3\rangle$ and $|4\rangle$. Thus the system is indeed subject to some Doppler broadening , as opposed to conventional Doppler-free geometries where true two-photon pumping creates an intermediate excited level with zero recoil momentum [33].

A useful alternative picture of Doppler broadening has emerged from considering superradiant process in ultracold atomic gases [34, 35], based on the interplay between the spatial coherence length and the recoil velocity. In this picture, a thermal atom is viewed as a spatial 'blob' of coherence, whose size is given by the thermal coherence length $\lambda_{coh} = \hbar/\sqrt{2mk_BT}$. When a single photon is *collectively* absorbed, each atom is placed in a quantum superposition of its initial state, and the excited state, which is also a coherent blob, but one which is moving at the recoil velocity relative to the initial blob. If collective excitation lives too long, then the initial and excited coherence blobs no longer overlap in *space*, at which point it no longer matters whether or not they overlap in momentum space. Overlap in both momentum and position space is required in order for the 'which-atom' information to be erased. This sets a minimum criterion for collective effects as, $v_r\tau_c \ll \lambda_{coh}$, where $v_r = \hbar K/M$ is the recoil velocity, and $\tau_c$ is lifetime of the collective excitation. With $\Gamma_c = 1/\tau_c$, this gives $\Gamma_c \gg \Gamma_d(T)$ as the necessary condition for collective enhancement, where

$$\Gamma_d(T) = K\sqrt{\frac{k_BT}{m}}, \tag{22}$$

is the usual Doppler broadening contribution the linewidth. We therefore see that Doppler broadening becomes significant only when $\Gamma_d(T)$ is greater than or comparable with the linewidth of signal and idler photons, both given by $D\,\Gamma_4$. The threshold temperature of the system is then determined as

$$T_c = \frac{mD^2\Gamma_4^2}{k_B|\mathbf{K}|^2}, \tag{23}$$

above which collective effects disappear. Taking typical $|\mathbf{K}| = 10^7\mathrm{m}^{-1}$, $D = 100$ and $m = 10^{-25}$kg, for $\Gamma_4 = 10^6\mathrm{s}^{-1}$, $10^7\mathrm{s}^{-1}$, and $10^8\mathrm{s}^{-1}$, we have $T_c = 10$, $10^2$, and $10^4$ kelvin, respectively. Due to the scaling of $T_c$ as $\Gamma_4^2$, we see that there could be a significant advantage to using an atomic transition with a large natural linewidth.

This means the present butterfly scheme can be implemented with room-temperature atomic clouds, excluding Cs which has $\Gamma \sim 10^6$, and so must be cooled below 10K. We note that at intermediate temperature, defined as $D\,\Gamma_4 > \Gamma_d(T) \gg \sqrt{\Delta^2 + \Gamma_2^2}$, where $\Delta$ is the detuning of $\Omega_d$ (which so far is taken to be zero), the effective linewidth of level $|2\rangle$ is broadened from $\Gamma_2$ to $\Gamma_d(T)$. For $\Delta = 0$, this is the case when $T \gtrsim 1$ kelvin. The only consequences of this, however, are that the various laser intensities and detunings would have to be adjusted accordingly to maintain the condition (10), and the sum-frequency linewidth would be similarly Doppler broadened. The pair correlations, however, will be unaffected. In contrast, for $T > T_c$ the pairing effect will completely disappear.

## III. REALISTIC MODELS

In the above section, we used a simplified toy model to illustrate the physics of the butterfly scheme for ultrabright photon pairs. In this section, we provide two realizations of the butterfly scheme, implemented with Ytterbium (section III A) and Cesium atoms (section III B), respectively. The main difference between toy and realistic models is that in the toy model, we use effective Rabi frequencies to describe the multi-photon pumping dynamics. In practice, this is an over-simplification of a complex dynamical process, and excludes the background Rayleigh/Raman scatterings associated with the intermediate states. To study these features, in the following section, we shall expand the toy dynamical model to account fully for the multi-photon nature of the drive and control fields.

### A. Ytterbium Atoms

We now consider a realistic butterfly level scheme configured on the 399nm-line of the $6s^2\ {}^1\mathrm{S}_0 \leftrightarrow 6s6p\ {}^1\mathrm{P}_1$ transition in $^{171}$Yb atoms, as shown in figure 4 (a). The atoms are prepared in the $|1\rangle \equiv |F = 1/2, m_F = -1/2\rangle$ state and then follow a FWM cycle which deposits them in level $|3\rangle$. A second independent FWM cycle then returns them to the initial $|1\rangle$ state. The driving FWM cycle consists of one violet laser and two infrared lasers, with Rabi frequencies $\Omega_1$, $\Omega_2$ and $\Omega_3$. The coupling FWM cycle similarly contains one violet and two infrared lasers, with Rabi frequencies of $\Omega_4$, $\Omega_5$ and $\Omega_6$. The net momenta of the driving lasers are equal and opposite with that of coupling lasers. Signal photons are emitted as $|2\rangle \equiv |F = 3/2, m_F = 3/2\rangle$ atoms spontaneously decay to the only dipole-allowed state of $|3\rangle \equiv |F = 1/2, m_F = 1/2\rangle$, and idler photons are gen-

erated as each atom in $|4\rangle \equiv |F = 3/2, m_F = -3/2\rangle$ decays collectively back to $|1\rangle$ with initial momentum $\hbar\mathbf{k}_0$. Both transitions have a natural linewidth of 0.2 GHz. Atoms which spontaneously decay to other momentum modes of level $|1\rangle$ generate unpaired rogue photons. Yet, they are still able to participate in the next-round collective emission cycle. In contrast, atoms which spontaneously decay from the intermediate pump levels to $|3\rangle$ are not eligible for the collective emission. They nonetheless can be repumped back to $|1\rangle$ in subsequent dynamics, during which more rogue photons will be emitted. For simplicity, however, in the present model we treat all unpaired-emission events as permanent atom losses, thereby excluding any of the aforementioned recycling or repumping processes. We note here the background scatterings, involving spontaneous single-photon decay of $m_F = -1/2, 1/2$ hyperfine states of the $6s6p$ level, are efficiently suppressed by making $\Omega_1$ and $\Omega_4$ far-detuned from resonance. The intermediate $6s5d$ level has a long lifetime of 6700ns, compared to 5ns for the $6s6p$ level, so that the spontaneous decay is negligible.

In the present scheme, $\Omega_3$ and $\Omega_6$ correspond to identical but counterpropagating lasers, and are thus interchangeable. In the driving process from $|1\rangle$ to $|2\rangle$, an atom is equally likely to absorb a photon from either of the two lasers. Then, during the coupling from $|3\rangle$ to $|4\rangle$, it will preferably absorb a photon from the other laser, following by collectively decay. This is because for the competing process of absorbing a same-momentum photon, the phase matching condition for collectivity is not satisfied. Consequently, atoms driven by this channel only decay spontaneously, the rate of which is a factor $1/D \ll 1$ smaller than that of the collective, phase-matching channel.

The system's dynamics is solved by extending the rate equations (1)-(6) to include intermediate pumping levels, such as levels of $6s6p, m_F = -1/2, 1/2$ and $6s5d, m_F = -3/2, 3/2$, as well as important side transition channels, including atom loss from $|1\rangle$ due to excitation by laser $\Omega_4$ and $\Omega_5$. The resulting rate equations are obtained in a straightforward manner very similar to the Cesium example derived explicitly in the appendix B.

We consider a cold ($< 1$ kelvin) spherical cloud of $10^6$ atoms with diameter $L = 26$ $\mu$m, corresponding to an optical depth of $D = 20$. The six pumping lasers are chosen such that the Rabi frequencies and detunings of transitions denoted in Fig. 4 yield values of (all in units of GHz) $\Omega_1 = 5$, $\Omega_2 = 16$, $\Omega_3 = 2$, $\Omega_4 = 10$, $\Omega_5 = 35$, $\Omega_6 = 2$, $\Delta_1 = 1000$, $\Delta_2 = 1200$. With these parameter choices, the effective Rabi strength resonantly coupling $|1\rangle$ to the level of $|F = 3/2, m_F = 3/2\rangle$ is $\Omega_{\text{eff}} = \frac{\Omega_1\Omega_2}{2\Delta_1} = 0.04$GHz, obtained by adiabatically eliminating the intermediate $6s6p$ level using $\Omega_1, \Omega_2 \ll \Delta_1$. The same lasers couple $|1\rangle$ to another hyperfine level of $|c\rangle \equiv |F = 5/2, m_F = 3/2\rangle$, but blue detuned from resonance by $\Delta_{hf} = 4$GHz. The effective Rabi frequency is $\Omega_{\text{eff}}/2 \ll \Delta_{hf}$. This, aided by that the Rabi frequency between $|c\rangle$ and $|2\rangle$ is $2\Omega_3 \not> \Delta_{hf}$, suppresses the pumping from $|1\rangle$ to $|c\rangle$. This suppression necessarily provides a non-vanishing coupling channel from $|1\rangle$ to $|2\rangle$. Similarly, the coupling between $|3\rangle$ and $|f\rangle \equiv |F = 5/2, -3/2\rangle$, yielding an effective Rabi frequency of $0.14\text{GHz} \ll \Delta_{hf}$, is suppressed, too. We have numerically verified this analysis, where the population ratio between level $|b\rangle \equiv |F = 3/2, m_F = 3/2\rangle$ and $|c\rangle$ is found to be 4, while the ratio between $|e\rangle \equiv |F = 3/2, m_F = -3/2\rangle$ and $|f\rangle$ is 14.

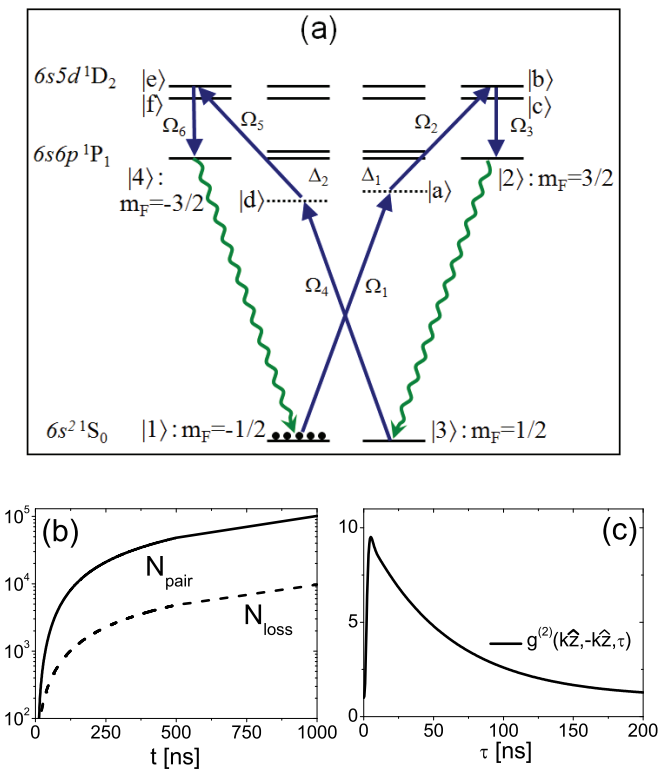


FIG. 4: (Color online) A realistic butterfly scheme using $^{171}$Yb atoms. Similarly to figure 5 for Cesium atoms, figure (a) shows the level diagram, (b) plots the time evolutions of $N_{pair}$ and $N_{loss}$, and (c) draws the time correlation function.

With the above observations, we have solved the extended rate equations numerically, with results shown in figure 4 (b) and (c). In figure (b), the production rate of photon pairs is about $10^{11}$ per second, while the atom loss from initial momentum modes is about $10^{10}\text{s}^{-1}$. The ratio of generated pairs $N_{pair}$ to lost atoms $N_{loss}$ is then 10. In figure (c), the time correlation function exhibits sharp peaks, showing strong pair correlation between signal and idler photons. The bandwidth of signal and idler photons, measured by the reciprocal of correlation time, is about 15MHz, much smaller than the natural linewidth $\Gamma_4 = 0.2$GHz. This is because the coupling between $|3\rangle$ and $|4\rangle$ is much weaker than the collective decay, so that the system dynamics is in the overdamped regime.

The major atom loss is attributed to $|1\rangle$ atoms being off-resonantly pumped to excited levels by $\Omega_1$ and

$\Omega_4$, and then decaying non-collectively by emitting rogue photons. These rogue photons are different in frequency from signal and idler photons by $\sim$ 1000 GHz, which is much larger than the bandwidth of single and idler photons ($\sim$ 0.02GHz). They can thus be easily filtered out from the photon-pair beams by optical frequency-selectors, and therefore will not contribute to the impurity of collected biphoton beams. By excluding such rogue photons, the ratio of "good" paired photons to the remaining rogue photons, which are nearly frequency-degenerate with the photon pairs, turns out to be around 20. For a twin beam of $N$ pairs, this results in a fluctuation of $\sqrt{N/20}$ in the number difference between the two beams. In contrast, the number-difference fluctuation for two uncorrelated coherent beams of the same size is $\sqrt{2N}$. Hence, the generated twin beams in the present setup yield a considerable number-squeezing factor of $\sqrt{2N}/\sqrt{N/20} = 2\sqrt{10}$.

### B. Cesium Atoms

We now consider another implementation configured on the 852-nm line of D2 transition in Cesium atoms. The $|1\rangle$, $|2\rangle$, $|3\rangle$ states are corresponding to $|F = 3, m_F = 3\rangle$, $|F = 5, m_F = 5\rangle$, $|F = 4, m_F = 4\rangle$ levels, respectively. State $|4\rangle$ is consisted of degenerate $|F = 4, m_F = 4\rangle$ and $|F = 5, m_F = 4\rangle$ hyperfine levels. Driving from $|1\rangle$ to $|2\rangle$ is accomplished via a FWM process, through detuned intermediate levels of $6P_{3/2}$ and $6D_{5/2}$. The three driving lasers, with Rabi frequencies $\Omega_1$, $\Omega_2$ and $\Omega_3$, are $\pi$, $\sigma_+$ and $\sigma_-$ polarized, respectively. In order to match the frequencies of signal and idler photons, the $\Omega_3$ laser is blue-detuned by the ground hyperfine splitting of 9.2 GHz. We note since the lifetime of the $6D_{5/2}$ level ($\sim$ 1 $\mu$s) is about 30 times longer than that of $6p_{3/2}$ ($\sim$ 30 ns), $\Omega_2$ can be tuned near- or on- resonant without resulting in a faster atom loss than the photon-pair gain. The coupling between $|3\rangle$ and $|4\rangle$ is provided by a single resonant $\pi$-laser. Signal photons are emitted as $|2\rangle$ atoms spontaneously decay to $|3\rangle$, while idler photons are generated as $|4\rangle$ atoms collectively decay back to $|1\rangle$. Thus different from the toy level scheme plotted in Fig. 1 and the Ytterbium scheme shown in Fig. 4, the emitted photon pairs now have the same polarizations. Collecting these pairs directly generates a highly spin-squeezed beam in twin-Fock state, which is potentially useful for precision interferometry measurement at Heisenberg-limited sensitivity [36, 37], as well as on-demand quantum teleportation among single-atom qubits [38].

The system's dynamics is solved by extending the rate equations (1)-(6) to include all intermediate pumping levels, such as levels $|a\rangle \equiv |6P_{3/2}, m_F = 3\rangle$ and $|b\rangle \equiv |6D_{5/2}, m_F = 4\rangle$, as shown in figure 5 (a). Each level is associated with a corresponding spontaneous decay rate to account for background Rayleigh and/or Raman scattering of pumping lasers. Furthermore, there exist undesired side transitions due to cross-driving by pumping lasers. For example, atoms in $|1\rangle$ state are also driven by the $\Omega_4$ laser to excited states, and $|3\rangle$ atoms are additionally coupled to $|4\rangle$ by the $\Omega_1$ laser. These transition are, however, far detuned from resonance. The net effects are then atom losses from relevant levels, and can thus be conveniently included in the rate-equation model by adding appropriate loss rates to corresponding levels. In this way, the multi-photon nature of driving and/or coupling is exactly treated via a dynamical model, while the background scatterings involving side transitions are calculated in a semi-exact manner, whose validity is justified by large detunings. We present the extended set of rate equations for the present Cesium scheme in appendix B.

To examine the performance of the Cesium scheme, we consider a spherical cloud of $10^6$ atoms with a diameter of $L = 44$ $\mu$m, corresponding to $D = 30$. The temperature of the cloud is assumed to be well below 1 kelvin, so that Doppler broadening of level $|2\rangle$ is negligible compared to its natural linewidth. We choose the pumping parameters as (all in units of GHz): $\Omega_1 = 2$, $\Omega_2 = 100$, $\Omega_3 = 20$, $\Omega_4 = 0.25$, $\Delta_1 = 300$, $\Delta_2 = 5$, $\Delta_3 = 9.2$. We numerically solve the extended rate equations, with results shown in figure 5 (b) and (c). In figure (b), the production rate of photon pairs is $1.7 \times 10^{11}$ per second, while the atom loss rate is $0.2 \times 10^{11}\text{s}^{-1}$. The photon-pair gain to atom loss ratio is then $\sim 9$. In figure (c), the time correlation function exhibits sharp peaks, indicating strong pair correlation between signal and idler photons. The bandwidth of signal and idler photons, measured by the reciprocal of correlation time, is about 100MHz, which is larger than the corresponding natural linewidth of 33 MHz.

For the present setup, there are three dominating atom loss channels. The first is via spontaneous relaxation of atoms in the intermediate pumping level $|6D_{5/2}, m_F = 4\rangle$, imparting emitting rogue photons at 917nm wavelength. The second is via background Rayleigh and/or Raman scattering of the $\Omega_1$ laser by the populated $|1\rangle$ level, emitting photons at a frequency 300 GHz smaller than that of paired photons. The third channel is via spontaneous emission of $|4\rangle$ atoms to $|3\rangle$ and the ground $|F = 4, m_F = 3\rangle$ level, emitting rogue photons whose frequency is 9.2GHz smaller than the paired photons. All these frequency-differences are much larger than the bandwidth of generated photon pairs ($\sim$ 0.1GHz), and can thus be filtered out by optical frequency-selectors. By excluding the aforementioned rogue photons, the ratio of "good" paired photons to the remaining rogue photons in the collected biphoton beams turns out to 25, corresponding to a considerable squeezing factor of $5\sqrt{2}$.

## IV. REABSORPTION ANALYSIS

In any scheme using atomic ensembles for biphoton sources, photon pairs are generated inside an optically-thick atomic cloud. This raises the question of whether or not they are able to propagate out of the cloud with-

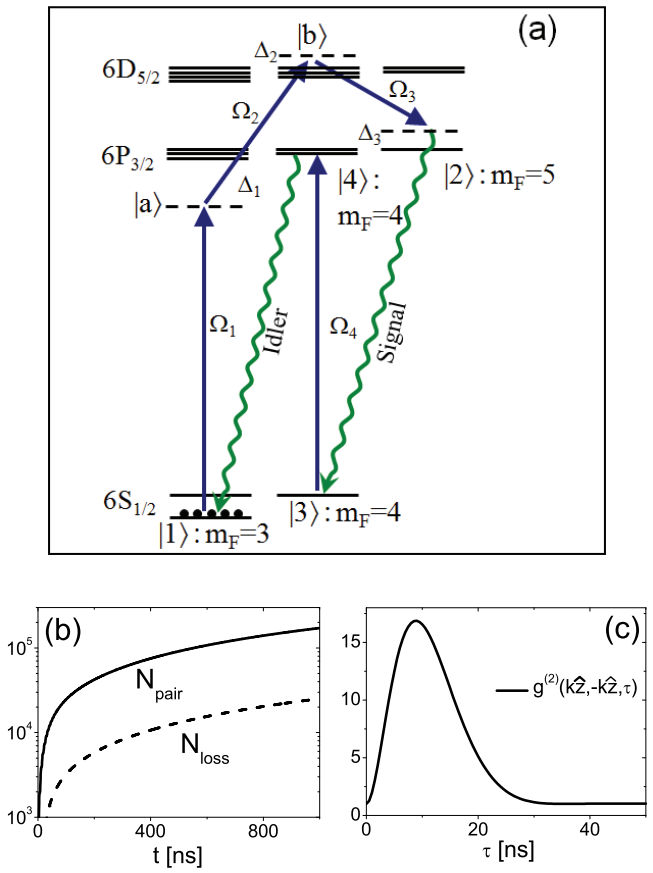


FIG. 5: (Color online) A realistic butterfly scheme using Cesium atoms. Figure (a) shows the level diagram, (b) plots $N_{pair}$ and $N_{loss}$, and (c) shows the time correlation function for photon pairs emitted along $\pm\hat{z}$ directions

out reabsorption. In some schemes [15, 18, 22], suppression of this reabsorption occurs naturally, due to the existence of an inherent electromagnetically-induced transparency (EIT) window [2, 8, 39]. For example, in Ref. [22], where the generated photon pairs yield narrow, sub-natural bandwidths due to overdamped coupling, the idler photons are shown to propagate within the systems EIT window, thus suppressing the reabsorption. The signal photons, on the other hand, are off-resonance with respect to excitation of the only populated $|1\rangle$ level, and thus in fact "see" an optically thin medium.

In the Ytterbium scheme, similar EIT windows exist for both signal and idler photons as well. For signal photons, the EIT window is formed by the $|1\rangle \leftrightarrow |a\rangle \leftrightarrow |^1\mathrm{D}_2, m_F = 1/2\rangle$ $\Lambda$-structure. The signal photons weakly drive the $|1\rangle \leftrightarrow |a\rangle$ transition, while the resonant laser $\Omega_3$ strongly drives the $|a\rangle \leftrightarrow |^1\mathrm{D}_2, m_F = 1/2\rangle$ transition. Since i) the $^1\mathrm{D}_2$ level (with a lifetime of 6700ns) is practically metastable compared to $^1\mathrm{P}_1$ (with a lifetime of 5ns), and ii) the couplings of $^1\mathrm{D}_2$ to other levels are negligibly weak compared to $\Omega_3$, the present $\Lambda$-structure is effectively mapped onto the three-level EIT model [15, 18, 22]. For idler photons, similar arguments apply, with the EIT window formed by the $|1\rangle \leftrightarrow |4\rangle \leftrightarrow |e\rangle$ $\Lambda$-structure. These, together with the fact that the generated photon pairs yield a sub-natural bandwidth, give rise to similar EIT reabsorption-suppression effects demonstrated in previous experiments [18, 22], so that in the present setup the majority of signal and idler photons will be able to propagate out the atomic vapor.

In the Cesium scheme, the signal and idler photons, which are both frequency and polarization degenerate, identically 'see' a EIT window formed by the $|1\rangle \leftrightarrow |4\rangle \leftrightarrow |3\rangle$ $\Lambda$-structure, where the transition $|4\rangle \leftrightarrow |3\rangle$ is resonantly driven by the strong $\Omega_4$ laser, as in figure 5 (a). However, unlike the Ytterbium and previous schemes, here the bandwidth of photon pairs is of the order of $1/10\,\mathrm{ns} = 0.1\mathrm{GHz}$, as from figure 5 (c). This bandwidth is broadened from the natural linewidth 0.03GHz. Thus, it is unlikely that the EIT-suppression effect still applies, as the bandwidth of photon pairs now matches the transparency window. On the other hand, the pulse duration of the photon pairs is $(D\Gamma_4)^{-1}$, whereas any scattering event occurs at a rate not exceeding $\Gamma_4$. The probability for photon scattering is then upper-bounded by $(D\Gamma_4)^{-1}\Gamma_4 = 1/D \ll 1$. To verify this, in the following we use a simplified model to simulate the absorption of a single-photon pulse passing through a $\Lambda$-structure cloud. To account for the super-natural bandwidth of $D\,\Gamma_4$, we approximate the single-photon Rabi frequency $\Omega_y(t)$ with a "toy" envelope function of

$$\Omega_y(t) = \Omega_0 e^{-D\Gamma_4 t/2}\sin(\Omega_4 t/2) \tag{24}$$

where the coefficient

$$\Omega_0 = \frac{8\Gamma_2 D}{\Omega_4}\sqrt{\frac{D^2\Gamma_4^2 + \Omega_4^2}{N\pi}} \tag{25}$$

is determined such that the underlying EM field yields the single-photon energy $\hbar c|\mathbf{K}|$. The atomic dynamics of this $\Lambda$ system is governed by a set of rate equations,

$$\frac{d}{dt}N_1 = \frac{i}{2}(\Omega_y\varrho_{41} - c.c) + \Gamma_{41}\bar{\beta}N_4(N_1+1), \tag{26}$$

$$\frac{d}{dt}N_3 = \frac{i}{2}(\Omega_4\varrho_{43} - c.c) + \Gamma_{43}\bar{\beta}N_4(N_3+1), \tag{27}$$

$$\frac{d}{dt}N_4 = -\frac{i}{2}(\Omega_4\varrho_{43} + \Omega_y\varrho_{41} - c.c) - \Big(\Gamma_4 + \bar{\beta}(\Gamma_{41}N_1 + \Gamma_{43}N_3)\Big)N_4, \tag{28}$$

$$\frac{d}{dt}\varrho_{41} = -i\frac{\Omega_y}{2}(N_4 - N_1) + i\frac{\Omega_4}{2}\varrho_{31} - \left(\frac{\Gamma_4}{2} - \frac{\Gamma_{41}}{2}\bar{\beta}(N_4 - N_1) + \frac{\Gamma_{43}}{2}\bar{\beta}N_3\right)\varrho_{41}, \quad (29)$$

$$\frac{d}{dt}\varrho_{43} = -i\frac{\Omega_4}{2}(N_4 - N_3) + i\frac{\Omega_y}{2}\varrho_{31}^* - \left(\frac{\Gamma_4}{2} - \frac{\Gamma_{43}}{2}\bar{\beta}(N_4 - N_3) + \frac{\Gamma_{41}}{2}\bar{\beta}N_1\right)\varrho_{43}, \quad (30)$$

$$\frac{d}{dt}\varrho_{31} = -i\frac{\Omega_y}{2}\varrho_{43}^* + i\frac{\Omega_4}{2}\varrho_{41} + \left(\frac{\Gamma_{43} + \Gamma_{41}}{2}\bar{\beta}N_4\right)\varrho_{31}, \quad (31)$$

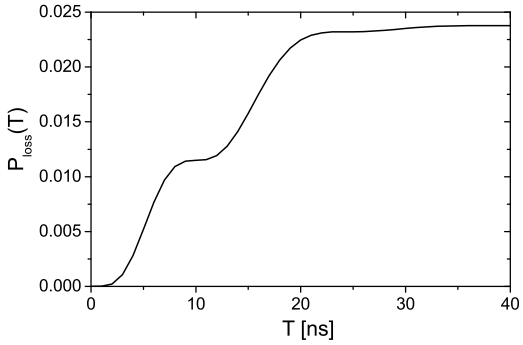


FIG. 6: The loss probability $P_{loss}(T)$ as a function of time $T$ for both signal and idler photons in the cesium scheme.

obtained in a similar manner with Eq. (1)-(6). Here, $N_1$, $N_3$ and $N_4$ are populations at level $|1\rangle$, $|3\rangle$ and $|4\rangle$. $\varrho_{ij}$ $(i, j = 1, 3, 4)$ is the coherence between level $|i\rangle$ and $|j\rangle$. $\Gamma_{ij}$ is the spontaneous emission rate from $|i\rangle$ to $|j\rangle$ and $\Gamma_i = \sum_j \Gamma_{ij}$ is the natural linewidth of level $|i\rangle$. Starting with all atoms in the $|1\rangle$ state, the above equations of motion are solved numerically. Because photon losses correspond to scattering atoms out of the $\Lambda$ system, the loss probability $P_{loss}$ of the photon passing through the medium is given by the atomic population reduction,

$$P_{loss}(T) = N_1\Big|_{t=0} - (N_1 + N_2 + N_3)\Big|_{t=T}. \quad (32)$$

A plot of $P_{loss}(T)$ is shown in figure 6, for parameters used in section III B. We find the ultimate loss probability $P_{loss}(\infty) \approx 0.02$ for both signal and idler photons. This result is consistent with the upper-limit of $1/D \approx 0.03$ as from the time-scale argument. In practice, this photon loss due to absorption will lead to a 2% degradation of the pair correlation.

## V. CONCLUSION AND DISCUSSIONS

In this paper we have proposed an omnidirectional biphoton source based on collective emission in an atomic vapor. This is accomplished by employing multi-photon excitation and 'Doppler-free' pumping. Our scheme benefits from the elimination of background Rayleigh scattering via dipole-selection rules, and the fact that phase-matching can be fullfilled in the full $4\pi$ solid angle. We have demonstrated an achievable photon-pair brightness of several orders of magnitude greater than the best reported results. Our scheme has the unique feature of strongly suppressed atomic re-thermalization, thus allowing implementations in 'hot' vapors as well as ultracold samples such as BEC's, performed nondestructively. This may lead to nondestructive *in situ* imaging of condensates, with an anticipated atom-counting precision below the standard quantum limit. This is because potentially, more photons than atoms can be generated before destroying the condensate. Furthermore, we found strong time and polarization correlation between signal and idler photons. We also provided two realistic implementation of the present scheme, using Cesium and Ytterbium atoms. In both schemes, the generated photon pairs can propagate through the optically thick cloud without being reabsorbed.

In the present scheme, the impurity of collected biphoton beams are attributed to i) non-collective emissions from level $|4\rangle$, and ii) background Raman/Rayleigh scattering of pumping lasers by the $|1\rangle$ atoms. The branch ratio of collective to non-collective emission is $D$, i.e., the optical depth of the atomic sample. One then might seek to improve the beam purity by employing samples of higher optical depth. The difficulty is that this requires a stronger coupling between $|3\rangle$ and $|4\rangle$, in order to maintain a strong time correlation between signal and idler photons. In both Yb and Cs schemes, this will unavoidably lead to a stronger background scattering, adding to the beam impurity.

Hence, an optimal optical depth is in fact obtained by balancing the two impurity sources of non-collective emission from level $|4\rangle$ and Raman/Rayleigh scattering of pumping lasers by the $|1\rangle$ atoms. To strongly drive the $|3\rangle \leftrightarrow |4\rangle$ transition while avoiding significant background scattering, it is clearly necessary to seek appropriate level structures where the coupling is resonant for the $|3\rangle \leftrightarrow |4\rangle$ transition, but far detuned from exciting $|1\rangle$ atoms. An example is seen in the Cesium scheme in section III B, where the coupling laser $\Omega_4$, while resonant with the $|3\rangle \leftrightarrow |4\rangle$ transition, is red-detuned from the $|1\rangle$ excitation due to ground hyperfine splitting. For further improvements, one may seek level scheme configured on the fine structure to exploit the extremely large level splitting ($\gtrsim$ THz). Feasible atomic species include those having no ground state hyperfine splittings,

such as $^{120}$Sn and $^{28}$Si. For these atoms, we have found butterfly level structures similar to the cesium scheme shown in figure 5 (a), but configured on fine structure levels, where the spacing between level $|1\rangle$ and $|3\rangle$ is now $10^4 \sim 10^5$ GHz, instead of 9.2 GHz as for Cesium. These schemes are expected to have very low background scattering. The disadvantage, however, is that because the omnidirectional phase-matching condition relies on producing (nearly) identical-wavelength signal and idler photons, the $|2\rangle$ level must be blue-detuned by an amount of ground fine splitting of $10^4 \sim 10^5$ GHz, which would then require ultra-intense driving lasers, making it difficult implement a cw scheme experimentally. Future work will therefore study the feasibility and applicability of a pulsed driving scheme.

If desired, level structures similar to the Cesium scheme in figure 5 (a) can be applied to other Alkaline atoms, such as Rb and Na. However, they have smaller ground hyperfine splittings than Cs, and will thus be subject to stronger background scattering. To overcome this difficulty, one possibility would be to increase the splitting by applying a static magnetic field, making use of the fact that level $|1\rangle$ and $|3\rangle$ are exposed to different Zeeman shifts. For a rough estimation, increasing the splitting to 10 GHz only requires a magnetic field of $\sim 0.1$ T, suggesting experimental feasibility.

Lastly, we note that as the atom loss fraction becomes significant, the system will enter a more complicated regime, where the system tries to equilibrate, potentially resulting in macroscopic occupation of all ground hyperfine sub-levels, and presumably strongly diminished pair correlations. If this is the case, only a small number of photon pairs will be generated, but in a very short bright initial burst. Thus, the butterfly system may be an excellent source for generating highly number-difference squeezed twin pulses for quantum interferometry. Further studies of the butterfly system in this equilibrium regime remain as a future task.

Acknowledgement: we thank A. Leanhardt for helpful discussions. This work is supported in part by National Science Foundation Grant No. PHY0653373.

## APPENDIX A: DERIVATION OF RATE EQUATIONS

In this appendix, we describe how one can derive the rate equations (1)-(6) from first principles, based on a Markovian treatment of the optical field. We begin by deriving a coarse-grained version of the Heisenberg equation of motion for an arbitrary operator, $\hat{A}$. This approach is equivalent to the standard master equation approach, but eliminates the density operator, as it is an unnecessary intermediate step when the goal is to derive equations for expectation values of observables.

The standard quantum time propagator is given by $\hat{U}(t) = e^{-i\hat{H}t}$. Defining in the usual way, the Heisenberg picture operator, $\hat{A}(t,t_0) = \hat{U}^\dagger(t-t_0)\hat{A}\hat{U}(t-t_0)$, it the follows that $\hat{A}(t+\tau,t_0) = \hat{U}^\dagger(t+\tau-t_0)\hat{A}\hat{U}(t+\tau-t_0)$, so that

$$\begin{aligned}\frac{d}{dt}\hat{A}(t,t_0) &= \lim_{\tau\to 0}\frac{1}{\tau}\Big(\hat{U}^\dagger(t+\tau-t_0)\hat{A}\hat{U}(t+\tau-t_0) \\ &- \hat{U}^\dagger(t-t_0)\hat{A}\hat{U}(t-t_0)\Big) \qquad \text{(A1)}\end{aligned}$$

We can then set $t_0 = t$ to arrive at

$$\frac{d}{dt}\hat{A} = \frac{\hat{U}^\dagger(\tau)\hat{A}\hat{U}(\tau) - \hat{A}}{\tau} \qquad \text{(A2)}$$

where $\hat{A}$ is now the Schrödinger picture operator, and $\tau$ must be chosen sufficiently small. Taking the expectation value of this equation with respect to the state of the system at time $t$, will then yield the time-derivative of the expectation value at time $t$. The Markov approximation then consists of letting $\tau$ be small compared to the system evolution timescale, but long compared to the dephasing time of the reservoir.

Using this approach, we now derive a generic equation of motion for the toy level scheme of Sec. II A. We start from a generic system-reservoir model,

$$\hat{H} = \hat{H}_s + \hat{H}_r + \hat{V}_{sr}, \qquad \text{(A3)}$$

where the reservoir consists of a bath of bosonic field modes, governed by a Hamiltonian of the form

$$\hat{H}_r = \sum_{\mathbf{k}}(\omega_{\mathbf{k}} - \omega_s)\hat{a}^\dagger_{\mathbf{k}}\hat{a}_{\mathbf{k}}, \qquad \text{(A4)}$$

where $\hat{a}_{\mathbf{k}}$ annihilates a bath particle with wave-vector, $\mathbf{k}$, and frequency, $\omega_{\mathbf{k}}$, and $\omega_s$ is the resonance frequency for the system-reservoir interaction. We assume an interaction operator of the form

$$\hat{V}_{sr} = \sum_{\mathbf{k}} g_{\mathbf{k}}\hat{a}^\dagger_{\mathbf{k}}\hat{c}_{\mathbf{k}} + h.c., \qquad \text{(A5)}$$

where $\hat{c}_{\mathbf{k}}$ is an unspecified system operator.

Now let us evaluate (A2) for the case $\hat{A} \to \hat{S}$, where $\hat{S}$ is a system operator only. To second-order in $\hat{V}_{sr}$, this gives

$$\frac{d}{dt}\hat{S} = \frac{1}{\tau}\left[\hat{U}_0^\dagger(\tau)\hat{S}\hat{U}_0(\tau) - \hat{S}\right] + \frac{1}{\tau}\int_0^\tau dt_2\int_0^\tau dt_1\hat{U}_0^\dagger(t_1)\hat{V}_{sr}(t_1)\hat{U}_0^\dagger(\tau-t_1)\hat{S}\hat{U}_0(\tau-t_2)\hat{V}_{sr}(t_2)\hat{U}_0(t_2)$$

$$- \frac{1}{\tau}\int_0^\tau dt_2 \int_0^{t_2} dt_1 \hat{U}_0(\tau - t_2)\hat{S}\hat{U}_0(\tau - t_2)\hat{V}_{sr}(t_2)\hat{U}_0(t_2 - t_1)\hat{V}_{sr}(t_1)\hat{U}_0(t_1)$$
$$- \frac{1}{\tau}\int_0^\tau dt_2 \int_0^{t_2} dt_1 \hat{U}_0^\dagger(t_1)\hat{V}_{sr}(t_1)\hat{U}_0^\dagger(t_2 - t_1)\hat{V}_{sr}(t_2)\hat{U}_0^\dagger(\tau - t_2)\hat{S}\hat{U}_0(\tau) \quad \text{(A6)}$$

where $U_0(t) = e^{-i(H_s+H_r)t}$, and we have neglected the first-order terms as they will vanish when we trace over the reservoir degrees of freedom. For the Markov approximation, we first take

$$U_0(\tau) \approx (1 - i\tau\hat{H}_s)e^{-i\hat{H}_r\tau}, \quad \text{(A7)}$$

and then perform the reservoir trace. The time integrals are then handled via,

$$\int_0^{t_2} dt_1 e^{-i(\omega_{\mathbf{k}}-\omega_a)(t_1-t_2)} \approx \pi\delta(\omega_{\mathbf{k}} - \omega_a), \quad \text{(A8)}$$

which gives

$$\frac{d}{dt}\hat{S} = \sum_{\mathbf{k}} \pi\delta(\omega_{\mathbf{k}} - \omega_s)|g_{\mathbf{k}}|^2 \left[\left[\hat{c}_{\mathbf{k}}^\dagger, \hat{S}\right]\hat{c}_{\mathbf{k}} + \hat{c}_{\mathbf{k}}^\dagger\left[\hat{S}, \hat{c}_{\mathbf{k}}\right]\right] + i\left[\hat{H}_s, \hat{S}\right] \quad \text{(A9)}$$

If one desires, the equation of motion for the system density operator, $\hat{\rho}_s$, can be obtained as a special case of (A9), with the substitution $\frac{d}{dt} \to -\frac{d}{dt}$, as the state of the system must be evolved backwards in time to obtain the state in the Heisenberg picture.

For the toy model depicted in Fig. 1, the system Hamiltonian is

$$\hat{H}_s = \sum_{j=1}^N \left[\frac{\Omega_d}{2}\left(e^{i\mathbf{K}\cdot\hat{\mathbf{r}}_j}|2\rangle\langle 1|^{(j)} + e^{-i\mathbf{K}\cdot\hat{\mathbf{r}}_j}|1\rangle\langle 2|^{(j)}\right) + \frac{\Omega_c}{2}\left(e^{-i\mathbf{K}\cdot\hat{\mathbf{r}}_j}|4\rangle\langle 3|^{(j)} + e^{i\mathbf{K}\cdot\hat{\mathbf{r}}_j}|3\rangle\langle 4|^{(j)}\right)\right], \quad \text{(A10)}$$

where $\hat{\mathbf{r}}_j$ is the position operator of the $j^{th}$ atom, and the state $|m\rangle^{(j)}$ indicates that the $j^{th}$ atom is in internal state $|m\rangle$. The system Hamiltonian (A10) is given for a frame rotating at the system resonance frequency, $\omega_s$, corresponding to the frequency of the $|4\rangle \to |1\rangle$ and $|2\rangle \to |3\rangle$ transitions. The system-reservoir interaction is described by the system operators

$$\hat{c}_{\mathbf{k}} := \sum_{j=1}^N e^{-i\mathbf{k}\cdot\hat{\mathbf{r}}_j}\left(|1\rangle\langle 4|^{(j)} + |3\rangle\langle 2|^{(j)}\right). \quad \text{(A11)}$$

For the initial state of the system, we assume that each atom is an internal state $|1\rangle$, and occupies a single box eigenstate, $\mathbf{q}$, so that

$$|\psi_i\rangle = \prod_{j=1}^N |\mathbf{q}_j\rangle^{(j)} \otimes |1\rangle^{(j)}. \quad \text{(A12)}$$

The initial momentum of the $j^{th}$ atom, $\mathbf{q}_j$ is to be chosen at random from the Boltzman distribution. For large enough $N$, this will reproduce the results of thermal averaging in a single realization. We then introduce the set of states

$$|u_{\mathbf{q}1}\rangle^{(j)} := |\mathbf{q}_j + \mathbf{q}\rangle^{(j)} \otimes |1\rangle^{(j)} \quad \text{(A13)}$$
$$|u_{\mathbf{q}2}\rangle^{(j)} := |\mathbf{q}_j + \mathbf{K} + \mathbf{q}\rangle^{(j)} \otimes |2\rangle^{(j)}, \quad \text{(A14)}$$
$$|u_{\mathbf{q},3}\rangle^{(j)} := |\mathbf{q}_j + \mathbf{K} + \mathbf{q}\rangle^{(j)} \otimes |3\rangle^{(j)}, \quad \text{(A15)}$$
$$|u_{\mathbf{q}4}\rangle^{(j)} := |\mathbf{q}_j + \mathbf{q}\rangle^{(j)} \otimes |4\rangle^{(j)}, \quad \text{(A16)}$$

so that for the $j^{th}$ atom, $|u_{\mathbf{0}1}\rangle^{(j)}\rangle$ and $|u_{\mathbf{0}2}\rangle^{(j)}$ are the initial state and the state after interacting with the drive lasers, respectively. The states $|u_{\mathbf{q}3}\rangle^{(j)}$ and $|u_{\mathbf{q}4}\rangle^{(j)}$, then correspond to the state after emission of a signal photon with momentum $\mathbf{k} \approx -\mathbf{q}$, and the state after then absorbing a sequence of photons from the coupling lasers, respectively. Emission of an idler photon with $\mathbf{k} \approx \mathbf{q}$, will then return the atom to the $|u_{\mathbf{0}1}\rangle^{(j)}$; whereas emission of a rogue photon will transform the state into $|u_{\mathbf{q}1}\rangle$ with $\mathbf{q} \neq 0$.

With respect to the states (A13)-(A16), the system Hamiltonian becomes

$$\hat{H}_s = \sum_{\mathbf{q}}\left[\frac{\Omega_d}{2}\left(\hat{S}_{\mathbf{q}1\mathbf{q}2} + \hat{S}^\dagger_{\mathbf{q}1\mathbf{q}2}\right) + \frac{\Omega_c}{2}\left(\hat{S}_{\mathbf{q}3\mathbf{q}4} + \hat{S}^\dagger_{\mathbf{q}3\mathbf{q}4}\right)\right], \quad \text{(A17)}$$

where we have introduced the generic atomic transition operators,

$$\hat{S}_{\mu\nu} = \hat{S}^\dagger_{\nu\mu} := \sum_{j=1}^N |u_\mu\rangle\langle u_\nu|^{(j)}, \quad \text{(A18)}$$

where $\mu, \nu \in \{\{\mathbf{q}1\}, \{\mathbf{q}2\}, \{\mathbf{q}3\}, \{\mathbf{q}4\}\}$ are composite indices. Similarly, the interaction operators take the form

$$\hat{c}_{\mathbf{k}} = \sum_{\mathbf{q},\mathbf{Q}} f(\mathbf{k} + \mathbf{q} - \mathbf{Q})\left(\hat{S}_{\mathbf{q}1\mathbf{Q}4} + \hat{S}_{\mathbf{q}3\mathbf{Q}2}\right), \quad \text{(A19)}$$

where

$$f(\mathbf{k}+\mathbf{q}-\mathbf{Q}) = \langle\mathbf{q}|e^{-i\mathbf{k}\cdot\hat{\mathbf{r}}_j}|\mathbf{Q}\rangle = \frac{1}{V}\int_V d^3r\, e^{-i(\mathbf{k}+\mathbf{q}-\mathbf{Q})\cdot\mathbf{r}} \quad \text{(A20)}$$

is the static structure function of the sample.

The operators we are interested in are all one-body operators of the form (A18). In order to evaluate (A9) for these operators, we will need to evaluate commutators of the form,

$$\left[\hat{S}_{\mu\nu}, \hat{S}_{\alpha,\beta}\right] = \delta_{\nu,\alpha}\hat{S}_{\mu\beta} - \delta_{\mu,\beta}\hat{S}_{\alpha\nu}. \quad \text{(A21)}$$

Taking the expectation value of the equation of motion (A9) will then require us to compute the expectation value of the bilinear operator $\langle \hat{S}_{\mu\nu}\hat{S}_{\alpha\beta}\rangle$. Our strategy for dealing with these terms will make use of the underlying exchange symmetry which leads to the emergence of collectivity in the emission properties of the sample.

We note that the initial state (A12) is not symmetric under particle label exchange, due to the dependence of the state $|u_{\mathbf{0}1}\rangle^{(j)}$ on $\mathbf{q}_j$. However, as the set of states $\{|u_{\mathbf{q}1}\rangle^{(j)}, |u_{\mathbf{q}2}\rangle^{(j)}, \{|u_{\mathbf{q}3}\rangle^{(j)}\}, \{|u_{\mathbf{q}4}\rangle^{(j)}\}\}$ forms a complete basis, all expectation values of operators of the the form (A18) will depend only on inner-products of the form $\langle u_\mu|u_\nu\rangle^{(j)}$, which are in fact independent of the $\mathbf{q}_j$'s. For example, with $m, M \in \{1,2,3,4\}$, we have

$$\begin{aligned}\langle u_{\mathbf{q}m}|u_{\mathbf{Q}M}\rangle^{(j)} &= \langle m|^{(j)} \otimes \langle \mathbf{q}_j+\mathbf{q}|^{(j)}|M\rangle^{(j)} \otimes |\mathbf{q}_j+\mathbf{Q}\rangle^{(j)} \\ &= \delta_{m,M}\, f(\mathbf{q}-\mathbf{Q}) \qquad \text{(A22)}\end{aligned}$$

which does not depend on $\mathbf{q}_j$. This means that we can make any choice we like for the set of $\mathbf{q}_j$'s, without affecting the rate equation dynamics. We note that this occurs in part because we have neglected the kinetic energy of the atomic center-of-mass motion in our system Hamiltonian (A10), an approximation valid when the lifetime of a collective excitation is short compared to $1/(\omega_R+\Gamma_d(T))$, where $\omega_R = \hbar K^2/2M$ is the recoil frequency, and $\Gamma_d$ is the Doppler line-width (22).

One option is then to set all the $\mathbf{q}_j$'s to zero, in which case our initial state becomes explicitly symmetric under exchange of particle label exchange. Equivalently, one can recognize that the $\mathbf{q}_j$'s are redundant with the particle labels, so that exchange of the $\mathbf{q}_j's$ is part of the underlying symmetry. As the Hamiltonian is also symmetric under this form of particle exchange, it follows that the state of the full system will remain symmetric as it evolves in time. The full state of the system + reservoir can then be written as

$$|\psi_{SR}(t)\rangle = \sum_{\mu_1,\ldots,\mu_N}\sum_r c(\mu_1,\ldots,\mu_N;r)|u_{\mu_1}\rangle^{(1)} \otimes |u_{\mu_2}\rangle^{(2)} \otimes|u_{\mu_3}\rangle^{(3)}\ldots\otimes|u_{\mu_N}\rangle^{(N)}\otimes|r\rangle^{(R)}, \qquad \text{(A23)}$$

where $r$ is a composite index which sums over all states of the reservoir, and the state $|r\rangle^{(R)}$ lives in the reservoir Hilbert space. Particle exchange symmetry then requires that $c(\mu_1,\ldots,\mu_N;r)$ be invariant under exchange of any two $\mu_j$'s.

With the symmetric state (A23), we can now evaluate the expectation value of the product of two operators of the form (A18),

$$\langle \hat{S}_{\mu\nu}\hat{S}_{\alpha\beta}\rangle = \delta_{\nu\alpha}\langle \hat{S}_{\mu\beta}\rangle + \sum_{\substack{j,J=1\\J\neq j}}^{N}\langle \hat{S}^{(j)}_{\mu\nu}\hat{S}^{(J)}_{\alpha\beta}\rangle, \qquad \text{(A24)}$$

where

$$\hat{S}^{(j)}_{\mu\nu} := |u_\mu\rangle\langle u_\nu|^{(j)}, \qquad \text{(A25)}$$

and with $\mu = \mathbf{q}m$ and $\nu = \mathbf{Q}M$, we have introduced

$$\delta_{\mu\nu} = \delta_{\mathbf{q},\mathbf{Q}}\delta_{m,M}. \qquad \text{(A26)}$$

To illustrate an important consequence of exchange symmetry on the bilinear terms in (A24), we consider first the $j$=1, $J$=2 case,

$$\begin{aligned}\langle \hat{S}^{(1)}_{\mu\nu}\hat{S}^{(2)}_{\alpha\beta}\rangle &= \langle\psi(t)|\hat{S}^{(1)}_{\mu\nu}\hat{S}^{(2)}_{\alpha\beta}|\psi(t)\rangle \\ &= \sum_{\substack{\mu_1,\ldots,\mu_N\\ \nu_1,\ldots,\nu_N}}\sum_r c^*(\mu_1,\ldots,\mu_N;r)c(\nu_1,\ldots,\nu_N;r)\langle u_{\mu_1}|u_\mu\rangle\langle u_\nu|u_{\nu_1}\rangle\langle u_{\mu_2}|u_\alpha\rangle\langle u_\beta|u_{\nu_2}\rangle\langle u_{\mu_3}|u_{\nu_3}\rangle\ldots\langle u_{\mu_N}|u_{\nu_N}\rangle \\ &= \sum_{\mu_3,\ldots,\mu_N}\sum_r c^*(\mu,\alpha,\mu_3,\ldots,\mu_N;r)c(\nu,\beta,\mu_3,\ldots,\mu_N;r) \\ &= \sum_{\mu_3,\ldots,\mu_N}\sum_r c^*(\mu,\alpha,\mu_3,\ldots,\mu_N;r)c(\beta,\nu,\mu_3,\ldots,\mu_N;r) \\ &= \langle \hat{S}^{(1)}_{\mu\beta}\hat{S}^{(2)}_{\alpha\nu}\rangle, \qquad \text{(A27)}\end{aligned}$$

where we have used the relation $\langle u_\mu|u_\nu\rangle = \delta_{\mu,\nu}$ to eliminate these inner products. Because the state is symmetric under exchange of particle labels, Eq. (A27) can be generalized to $\langle \hat{S}^{(j)}_{\mu\nu}\hat{S}^{(J)}_{\alpha\beta}\rangle = \langle \hat{S}^{(j)}_{\mu\beta}\hat{S}^{(J)}_{\alpha\nu}\rangle$, for $j \neq J$, which gives us

$$\langle \hat{S}_{\mu\nu}\hat{S}_{\alpha\beta}\rangle = \delta_{\nu,\alpha}\langle \hat{S}_{\mu\beta}\rangle + \sum_{\substack{j,J=1\\J\neq j}}^{N}\langle \hat{S}^{(j)}_{\mu\beta}\hat{S}^{(J)}_{\alpha\nu}\rangle, \qquad \text{(A28)}$$

as an equivalent alternative to (A24). This result will allow us to express the equations of motion for number

operators in terms of products of number operators, as opposed to products of coherence operators.

The equation of motion for the expectation value of a system operator of the form (A18) is then

$$\frac{d}{dt}\langle\hat{S}_{\mu\nu}\rangle = \sum_{\mathbf{k}}\pi\delta(\omega_{\mathbf{k}}+\omega_s)|g_{\mathbf{k}}|^2\left(\langle\left[\hat{c}^\dagger_{\mathbf{k}},\hat{S}_{\mu\nu}\right]\hat{c}_{\mathbf{k}}\rangle + \langle\hat{c}^\dagger_{\mathbf{k}}\left[\hat{S}_{\mu\nu},\hat{c}_{\mathbf{k}}\right]\rangle\right) + i\langle\left[\hat{H}_s,\hat{S}_{\mu\nu}\right]\rangle. \tag{A29}$$

We can evaluate the commutators via Eqs. (A17), (A19) and (A21), resulting in

$$\left[\hat{c}^\dagger_{\mathbf{k}},\hat{S}_{\mu\nu}\right] = \sum_{\mathbf{q},\mathbf{Q}} f^*(\mathbf{k}+\mathbf{q}-\mathbf{Q})\left(\delta_{\mu,\mathbf{q}1}\hat{S}_{\mathbf{Q}4\nu} - \delta_{\nu,\mathbf{Q}4}\hat{S}_{\mu\mathbf{q}1} + \delta_{\mu,\mathbf{Q}2}\hat{S}_{\mathbf{q}3\nu} - \delta_{\nu,\mathbf{q}3}\hat{S}_{\mu\mathbf{Q}2}\right), \tag{A30}$$

$$\left[\hat{S}_{\mu\nu},\hat{c}_{\mathbf{k}}\right] = \sum_{\mathbf{q},\mathbf{Q}} f(\mathbf{k}+\mathbf{q}-\mathbf{Q})\left(\delta_{\nu,\mathbf{q}1}\hat{S}_{\mu\mathbf{Q}4} - \delta_{\mu,\mathbf{Q}4}\hat{S}_{\mathbf{q}1\nu} + \delta_{\nu,\mathbf{Q}2}\hat{S}_{\mu\mathbf{q}3} - \delta_{\mu\mathbf{q}3}\hat{S}_{\mathbf{Q}2\nu}\right). \tag{A31}$$

and

$$\left[\hat{H}_s,\hat{S}_{\mu\nu}\right] = \frac{\Omega_d}{2}\sum_{\mathbf{q}}\left(\delta_{\mu\mathbf{q}2}\hat{S}_{\mathbf{q}1\nu} - \delta_{\nu,\mathbf{q}1}\hat{S}_{\mu\mathbf{q}2} + \delta_{\mu,\mathbf{q}1}\hat{S}_{\mathbf{q}2\nu} - \delta_{\nu,\mathbf{q}2}\hat{S}_{\mu\mathbf{q}1}\right) + \frac{\Omega_c}{2}\sum_{\mathbf{q}}\left(\delta_{\mu\mathbf{q}4}\hat{S}_{\mathbf{q}3\nu} - \delta_{\nu,\mathbf{q}3}\hat{S}_{\mu\mathbf{q}4} + \delta_{\mu,\mathbf{q}3}\hat{S}_{\mathbf{q}4\nu} - \delta_{\nu,\mathbf{q}4}\hat{S}_{\mu\mathbf{q}3}\right) \tag{A32}$$

At this point, the variables used in the rate equations (1-6), can be precisely defined as

$$N_1 := \langle\hat{N}_{\mathbf{01}}\rangle = \langle\hat{S}_{\mathbf{0101}}\rangle, \tag{A33}$$

$$N_2 := \langle\hat{N}_{\mathbf{02}}\rangle = \langle\hat{S}_{\mathbf{0202}}\rangle, \tag{A34}$$

$$\varrho_{12} := \langle\hat{S}_{\mathbf{0102}}\rangle, \tag{A35}$$

$$N_{\mathbf{q}3} := \langle\hat{N}_{\mathbf{q}3}\rangle = \langle\hat{S}_{\mathbf{q}3\mathbf{q}3}\rangle, \tag{A36}$$

$$N_{\mathbf{q}4} := \langle\hat{N}_{\mathbf{q}4}\rangle = \langle\hat{S}_{\mathbf{q}4\mathbf{q}4}\rangle, \tag{A37}$$

$$\varrho_{\mathbf{q}34} = \langle\hat{S}_{\mathbf{q}3\mathbf{q}4}\rangle. \tag{A38}$$

The occupation numbers $N_1$ and $N_2$ count the number of atoms in internal states $|1\rangle$ and $|2\rangle$, respectively, that have not been 'lost' via emission of a rogue idler photon. The occupation numbers $N_{\mathbf{q}3}$ and $N_{\mathbf{q}4}$ count the number of atoms in internal states $|3\rangle$ and $|4\rangle$, which are displaced in momentum space by $\mathbf{K}+\mathbf{q}$ and $\mathbf{q}$, respectively, relative to their initial momenta, corresponding to their having emitted a signal photon with momentum $\mathbf{k}\approx-\mathbf{q}$. The coherence terms $\varrho_{12}$ and $\varrho_{\mathbf{q}34}$ describe the coherence generated by the driving and coupling lasers, respectively.

Beginning with $N_1$, we can derive its equation of motion from (A29) by setting $\mu=\nu=\mathbf{01}$. For the commutators (A30)-(A32) we find

$$\left[\hat{c}^\dagger_{\mathbf{k}},\hat{S}_{\mathbf{0101}}\right] = \sum_{\mathbf{q}} f^*(\mathbf{k}-\mathbf{q})\hat{S}_{\mathbf{q}4\mathbf{01}}, \tag{A39}$$

$$\left[\hat{S}_{\mathbf{0101}},\hat{c}_{\mathbf{k}}\right] = \sum_{\mathbf{q}} f(\mathbf{k}-\mathbf{q})\hat{S}_{\mathbf{01}\mathbf{q}4}, \tag{A40}$$

$$\left[\hat{H}_s,\hat{S}_{\mathbf{0101}}\right] = \frac{\Omega_d}{2}\left(\hat{S}_{\mathbf{0102}}-\hat{S}_{\mathbf{0201}}\right), \tag{A41}$$

which leads to

$$\frac{d}{dt}N_1 = \sum_{\mathbf{k}}\pi\delta(\omega_{\mathbf{k}}-\omega_s)|g_{\mathbf{k}}|^2\sum_{\mathbf{q},\mathbf{Q},\mathbf{Q}'} f^*(\mathbf{k}-\mathbf{q})f(\mathbf{k}+\mathbf{Q}'-\mathbf{Q})\left(\langle\hat{S}_{\mathbf{q}4\mathbf{01}}\hat{S}_{\mathbf{Q}'1\mathbf{Q}4}\rangle + \langle\hat{S}_{\mathbf{q}4\mathbf{01}}\hat{S}_{\mathbf{Q}'3\mathbf{Q}2}\rangle\right) - i\frac{\Omega_d}{2}\varrho_{12} + c.c. \tag{A42}$$

With the help of (A27) we see that

$$\langle\hat{S}_{\mathbf{q}4\mathbf{01}}\hat{S}_{\mathbf{Q}'1\mathbf{Q}4}\rangle = \delta_{\mathbf{Q}',0}\langle\hat{S}_{\mathbf{q}4\mathbf{Q}4}\rangle + \sum_{\substack{j,J=1\\J\neq j}}^{N}\langle\hat{S}^{(j)}_{\mathbf{q}4\mathbf{Q}4}\hat{S}^{(J)}_{\mathbf{Q}'1\mathbf{01}}\rangle. \tag{A43}$$

To implement the approximation that all atoms that emit rogue idler photons are permanently 'lost', we simply evaluate expectation values under the assumption that there are no atoms in the states $|u_{\mathbf{q}1}\rangle$ and $|u_{\mathbf{q}2}\rangle$ for $\mathbf{q}\neq0$. This allows us to make the simplifications

$$\langle\hat{S}_{\mathbf{q}4\mathbf{01}}\hat{S}_{\mathbf{Q}'1\mathbf{Q}4}\rangle = \delta_{\mathbf{Q}',0}\left(N_{\mathbf{q}4}+\langle\hat{N}_{\mathbf{q}4}\hat{N}_{\mathbf{01}}\rangle\right) \tag{A44}$$

and

$$\langle\hat{S}_{\mathbf{q}4\mathbf{01}}\hat{S}_{\mathbf{Q}'3\mathbf{Q}2}\rangle = \delta_{\mathbf{Q},0}\langle\hat{S}_{\mathbf{q}4\mathbf{01}}\hat{S}_{\mathbf{Q}'3\mathbf{02}}\rangle. \tag{A45}$$

Inserting these into (A43) and making the approximation

$$f^*(\mathbf{k}-\mathbf{q})f(\mathbf{k}-\mathbf{Q})\approx|f(\mathbf{k}-\mathbf{q})|^2\,\delta_{\mathbf{Q},\mathbf{q}}\,, \tag{A46}$$

then gives

$$\frac{d}{dt}N_1 = \frac{\Gamma}{2}\sum_{\mathbf{q}}\beta_{\mathbf{q}}\left(\langle\hat{N}_{\mathbf{q}4}\hat{N}_{\mathbf{01}}\rangle + N_{\mathbf{q}4} + \langle\hat{S}_{\mathbf{q}4\mathbf{01}}\hat{S}_{-\mathbf{q}3\mathbf{02}}\rangle\right) - i\frac{\Omega_d}{2}\varrho_{12} + c.c.\,, \tag{A47}$$

where we have introduced the branching ratio

$$\beta_{\mathbf{q}} := \frac{2}{\Gamma}\sum_{\mathbf{k}} \pi\delta(\omega_{\mathbf{k}}-\omega_s)|g_{\mathbf{k}}|^2|f(\mathbf{k}-\mathbf{q})|^2, \tag{A48}$$

where

$$\Gamma = \sum_{\mathbf{k}} 2\pi\delta(\omega_{\mathbf{k}}-\omega_s)|g_{\mathbf{k}}|^2 \tag{A49}$$

is the spontaneous emission rate for states $|2\rangle$ and $|4\rangle$, which we have implicitly set equal by making $\hat{c}_{\mathbf{k}}$ (A11) symmetric with respect to the two transitions.

The next step is to show that (a) $\langle \hat{N}_{\mathbf{q}4}\hat{N}_{\mathbf{0}1}\rangle \approx \langle \hat{N}_{\mathbf{q}4}\rangle\langle \hat{N}_{\mathbf{0}1}\rangle$, and (b) that $\langle \hat{S}_{\mathbf{q}4\mathbf{0}1}\hat{S}_{-\mathbf{q}3\mathbf{0}2}\rangle \ll \langle \hat{N}_{\mathbf{q}4}\hat{N}_{\mathbf{0}1}\rangle$, so that it can be safely neglected. In order to verify (a) and (b), it is useful to define the excitation-number operators

$$\hat{N}_{\mathbf{q}} := \hat{N}_{\mathbf{q}3} + \hat{N}_{\mathbf{q}4}. \tag{A50}$$

and

$$\hat{N}_e := \sum_{\mathbf{q}} \hat{N}_{\mathbf{q}}. \tag{A51}$$

with the number of non-excited atoms then given by

$$\hat{N}_0 := \hat{N}_1 + \hat{N}_2 = N - \hat{N}_e \tag{A52}$$

In terms of probabilities, the unproven approximation (a) can be re-expressed as

$$N(N-1)P_2(\mathbf{0}1,\mathbf{q}4) \approx N^2 P_1(\mathbf{0}1)P_1(\mathbf{q}4), \tag{A53}$$

where $P_2(\mu,\nu)$ is the joint probability that for any ordered pair of atoms, the first one will be in state $|u_\mu\rangle$ and the second in state $|u_\nu\rangle$, whereas $P_1(\mu) = N_\mu/N$ is the bare probability that any given atom will be in state $|u_\mu\rangle$. According to Bayes theorem, we have

$$P_2(\mathbf{q}4,\mathbf{0}1) = P_1(\mathbf{0}1|\mathbf{q}4)P_1(\mathbf{q}4) \tag{A54}$$

where $P_1(\mathbf{0}1|\mathbf{q}4)$ is the conditional probability to find a particular atom in state $|u_{\mathbf{0}1}\rangle$ given that another particular atom is in state $|u_{\mathbf{q}4}\rangle$. Knowing that the second atom is in state $|u_{\mathbf{q}4}\rangle$ means that of the remaining $N-1$ atoms, the average number of excited atoms is now $N_e - 1$, or equivalently, out of the remaining $N-1$ atoms, the average number in state $|u_{\mathbf{0}1}\rangle$ is still $N_1$, Thus we see that

$$P_1(\mathbf{0}1|\mathbf{q}4) = \frac{N_1}{N-1} = P_1(\mathbf{0}1)\frac{N}{N-1}. \tag{A55}$$

This leads to the result

$$\langle \hat{N}_{\mathbf{q}4}\hat{N}_{\mathbf{0}1}\rangle = \langle \hat{N}_{\mathbf{q}4}\rangle\langle \hat{N}_{\mathbf{q}}1\rangle, \tag{A56}$$

i.e. the factorization (a) is exact. We note that this would not be obtained without assuming a symmetrized wavefunction with fixed total atom number, which allowed us to replace (a) with Eq. (A53).

Turning now to the approximation (b), we begin by introducing the reduced two-body density operator

$$\rho_2(\mu,\alpha;\nu,\beta) := \langle \hat{S}_{\mu\nu}\hat{S}_{\alpha\beta}\rangle, \tag{A57}$$

so that $\langle \hat{S}_{\mathbf{q}4\mathbf{0}1}\hat{S}_{-\mathbf{q}3\mathbf{0}2}\rangle = \rho_2(\mathbf{q}4,-\mathbf{q}3;\mathbf{0}1,\mathbf{0}2)$. If we assume that the probability to have $N_{\mathbf{q}} > 1$ is negligible, it follows that the matrix element $\rho_2(\mathbf{q}4,-\mathbf{q}3;\mathbf{0}1,\mathbf{0}2)$ is a measure of the coherence between the $N_{\mathbf{q}} = N_{-\mathbf{q}} = 0$ manifold, and the $N_{\mathbf{q}} = N_{-\mathbf{q}} = 1$ manifold.

To understand the origin of such coherence in the system, let us start from the initial state $|\psi_i\rangle = \prod_{j=1}^{N}|u_{\mathbf{0}1}\rangle$, and assume that at time $t=0$, the driving and coupling laser beams are turned on. The atoms will adiabatically follow the ground state of the dressed system, so that immediately after the fields are turned on, the state of the system will be

$$|\psi_0\rangle = \prod_{j=1}^{N}\left(|u_{\mathbf{0}1}\rangle^{(j)} - i\frac{\Omega_d}{\Gamma}|u_{\mathbf{0}2}\rangle^{(j)}\right). \tag{A58}$$

This dressed state will decay by emitting a signal photons at the rate $\Gamma_{eff} = N\Omega_d^2/\Gamma$. The signal photons are distributed over the many recoil modes of the system, with branching ratio $\beta$ per mode. Thus from the perspective of a single $N_{\mathbf{q}}$ manifold, the time delay between signal photons is $T_0 = \beta/\Gamma_{err} = \Gamma/(\Omega_d^2 D)$, where we have used $D \approx N\beta$.

Let us assume that the first photon is emitted along $\mathbf{k} \approx -\mathbf{q}$, causing the system to jump from the $N_{\mathbf{q}} = N_{-\mathbf{q}} = 0$ manifold to the $N_{\mathbf{q}} = 1$, $N_{-\mathbf{q}} = 0$ manifold. The normalized state immediately after this quantum jump is given by

$$|\psi_1\rangle = \frac{\hat{c}_{-\mathbf{q}}|\psi_0\rangle}{\langle\psi_0|\hat{c}^\dagger_{-\mathbf{q}}\hat{c}_{-\mathbf{q}}|\psi_0\rangle^{1/2}}. \tag{A59}$$

By neglecting rogue-photon emission and making the approximation (A46), we can simplify (A19) to

$$\hat{c}_{\mathbf{q}} = \hat{S}_{\mathbf{0}1\mathbf{q}4} + \hat{S}_{-\mathbf{q}3\mathbf{0}2}, \tag{A60}$$

which leads to

$$|\psi_1\rangle = -i\frac{\Gamma}{\Omega_d N}\hat{S}_{\mathbf{q}3\mathbf{0}2}|\psi_0\rangle. \tag{A61}$$

This state will live for time $t_1 \sim T_e = \frac{1}{\Gamma D}$, after which a second photon will be emitted along the $\mathbf{k} \approx \mathbf{q}$ direction. With $t=0$ corresponding to the emission of the second photon, the state of the system at time $t$ later is then

$$|\psi_2(t)\rangle = \frac{U_c(t)\hat{c}_{\mathbf{q}}U_c(t_1)|\psi_1\rangle}{\langle\psi_1|U_c^\dagger(t_1)\hat{c}^\dagger_{\mathbf{q}}\hat{c}_{\mathbf{q}}U_c(t_1)|\psi_1\rangle^{1/2}}, \tag{A62}$$

where the propagator

$$U_c(t) = \exp\left[-i\frac{\Omega_c t}{2}\sum_{\mathbf{q}}\left(\hat{S}_{\mathbf{q}3\mathbf{q}4} + \hat{S}_{\mathbf{q}4\mathbf{q}3}\right)\right], \tag{A63}$$

describes the Rabi oscillations between states $|3\rangle$ and $|4\rangle$, that occur when $\Omega_c > \Gamma D/2$.

We can take $U_c(t_1)\hat{S}_{\mathbf{q}402} \approx \hat{S}_{\mathbf{q}402}$, as $U_c(t)$ mixes levels $|3\rangle$ and $|4\rangle$, and the highest probability of emission occurs when the excited atom is in level $|4\rangle$. This leads to the result

$$|\psi_2(t)\rangle \approx \frac{\Gamma}{\Omega_d N}\left(\hat{S}_{\mathbf{0}102} + U_c(t)\hat{S}_{-\mathbf{q}302}\hat{S}_{\mathbf{q}402}\right)|\psi_0\rangle, \tag{A64}$$

which shows that the state $|\psi_2(t)\rangle$ is in fact a coherent superposition of a state with $N_{\mathbf{q}} = N_{-\mathbf{q}} = 0$, corresponding to the second photon being an idler photon (emitted on the $|4\rangle \rightarrow |1\rangle$ transition) and a state with $N_{\mathbf{q}} = N_{-\mathbf{q}} = 1$, corresponding to the second photon being a new signal photon (emitted on the $|2\rangle \rightarrow |3\rangle$ transition). The lifetime of this coherent superposition state is $T_{coh} \sim T_e$, the timescale on which either (i) a second pair of photons will be emitted, confirming that the second photon was a signal photon, or (ii) no additional photons will be emitted, confirming that the second photon was the idler photon. In either case, the system will collapse back onto a state with $N_{\mathbf{q}} = N_{-\mathbf{q}} = 0$.

From this analysis, we now see that

$$\begin{aligned}\langle \hat{S}_{\mathbf{q}401}\hat{S}_{-\mathbf{q}302}\rangle &\approx \frac{T_e}{T_0}\langle\psi_2(t)|\hat{S}_{\mathbf{q}401}\hat{S}_{-\mathbf{q}302}|\psi_2(t)\rangle \\ &\approx \cos^2(\Omega_c t/2)\frac{\Omega_d^4}{\Gamma^4}N \end{aligned}\tag{A65}$$

where the factor $T_e/T_0 = \Omega_d^2/\Gamma^2$ is the probability to find the system in state $|\psi_2(t)\rangle$. To compare this to the term $\langle \hat{N}_{\mathbf{q}4}\hat{N}_{\mathbf{0}1}\rangle = N^2 P_1(\mathbf{0}1)P_1(\mathbf{q}4)$ in (A47), we need to estimate the single particle probabilities, $P_1(\mu)$. Estimates for these probabilites can be found from the equilibrium condition $R_s = R_I$. For $N_e \ll N$ and $\Omega_c \geq \Gamma D$, we can make the simple estimates $R_s = N_2\Gamma$ and $R_I = \frac{1}{2}N_e\Gamma D$. With $N_2 = \frac{\Omega_d^2}{\Gamma^2}N_1$ and $N_e = 1 - N_0$, we find $N_1 = \frac{\Gamma^2 N}{\Gamma^2+\Omega_d^2(1+2/D)}$, $N_2 = \frac{\Omega_d^2 N}{\Gamma^2+\Omega_d^2(1+2/D)}$, $N_e = \frac{(2/D)\Omega_d^2 N}{\Gamma^2+\Omega_d^2(1+2/D)}$, and $N_{\mathbf{q}3} \approx N_{\mathbf{q}4} \approx \frac{1}{2}\beta N_e$, which gives us

$$P_1(\mathbf{0}1) \approx 1 - \frac{\Omega_d^2}{\Gamma^2}, \tag{A66}$$

and

$$P_1(\mathbf{q}4) \approx \frac{\Omega_d^2}{\Gamma^2}\frac{1}{N}. \tag{A67}$$

Thus we see that

$$\langle \hat{N}_{\mathbf{q}4}\hat{N}_{\mathbf{0}1}\rangle \approx \frac{\Omega_d^2}{\Gamma^2}N, \tag{A68}$$

which is larger than $\langle \hat{S}_{\mathbf{q}401}\hat{S}_{-\mathbf{q}301}\rangle$ by a factor $(\Gamma/\Omega_d)^2$. For the parameters used in the numerical simulations of Sec. (II B), this is a factor of 100. Keeping only the dominant term, $\langle \hat{N}_{\mathbf{q}4}\hat{N}_{\mathbf{0}1}\rangle$, then leads to

$$\frac{d}{dt}N_1 = \Gamma\sum_{\mathbf{q}}\beta_{\mathbf{q}}N_{\mathbf{q}4}(N_1+1) - i\frac{\Omega_d}{2}\left(\varrho_{12} - c.c.\right), \tag{A69}$$

which for $\Gamma_4 = \Gamma$ and $\beta_{\mathbf{q}4} = \beta_{\mathbf{q}}$, validates the rate equation (1). Using the general methods outlined in this appendix, the remaining rate equations (2)-(6) can be derived as well. Clearly deriving these rate equations from first principles is highly non-trivial. However, once their validity is established, the fact that they follow an established form allows one to write them down directly, rather than re-derive them for each particular model.

## APPENDIX B: EXTENDED RATE EQUATIONS

In this section, we give the extended rate equations we have used to model the Cesium scheme presented in section III B. In the scheme, driving from $|1\rangle$ to $|2\rangle$ is accomplished via a three-photon process, through detuned intermediate levels of $|a\rangle \equiv |6P_{3/2}, m_F = 3\rangle$ and $|b\rangle \equiv |6D_{5/2}, m_F = 4\rangle$, as shown in figure 5 (a). With the conventions of $N_j$ being atom number in state $|j\rangle$ and $\varrho_{jh}$ being the coherence between $|j\rangle$ and $|h\rangle$, the equations are obtained as

$$\frac{d}{dt}N_1 = \frac{i}{2}\left(\Omega_1\varrho_{a1} - c.c\right) - \Gamma_1 N_1 + \alpha_{41}\Gamma_4^0\sum_{\mathbf{k}}\beta_{\mathbf{k}4}N_{\mathbf{k}4}(N_1+1), \tag{B1}$$

$$\frac{d}{dt}N_a = -\frac{i}{2}\left(\Omega_1\varrho_{a1} - c.c\right) + \frac{i}{2}\left(\Omega_2\varrho_{ba} - c.c\right) - \Gamma_a^0 N_a, \tag{B2}$$

$$\frac{d}{dt}N_b = -\frac{i}{2}\left(\Omega_2\varrho_{ba} - c.c\right) - \frac{i}{2}\left(\Omega_3\varrho_{b2} - c.c\right) - \Gamma_b^0 N_b, \tag{B3}$$

$$\frac{d}{dt}N_2 = \frac{i}{2}\left(\Omega_3\varrho_{b2} - c.c\right) - \Gamma_2\sum_{\mathbf{k}}\beta_{\mathbf{k}2}N_2(N_{\mathbf{k}3}+1), \tag{B4}$$

$$\frac{d}{dt}\varrho_{a1} = i\frac{\Omega_1}{2}(N_1 - N_a) + i\frac{\Omega_2}{2}\rho_{b1} + \left(i\Delta_1 - \frac{1}{2}(\Gamma_a^0 + \Gamma_1) + \frac{1}{2}\alpha_{41}\Gamma_4^0\sum_{\mathbf{k}}\beta_{\mathbf{k}4}N_{\mathbf{k}4}\right)\varrho_{a1} \quad \text{(B5)}$$

$$\frac{d}{dt}\varrho_{ba} = i\frac{\Omega_2}{2}(N_a - N_b) - i\frac{\Omega_1}{2}\varrho_{b1} + i\frac{\Omega_3}{2}\varrho_{a2}^* - \left(i(\Delta_2 + \Delta_1) + \frac{1}{2}(\Gamma_a^0 + \Gamma_b^0)\right)\varrho_{ba} \quad \text{(B6)}$$

$$\frac{d}{dt}\varrho_{b1} = i\frac{\Omega_2}{2}\rho_{a1} - i\frac{\Omega_1}{2}\varrho_{ba} + i\frac{\Omega_3}{2}\varrho_{21} + \left(\frac{1}{2}\alpha_{41}\Gamma_4^0\sum_{\mathbf{k}}\beta_{\mathbf{k}4}N_{\mathbf{k}4} - \frac{1}{2}(\Gamma_1 + \Gamma_b^0)\right)\varrho_{b1} + i\Delta_2\varrho_{b1}, \quad \text{(B7)}$$

$$\frac{d}{dt}\varrho_{b2} = i\frac{\Omega_3}{2}(N_2 - N_b) + i\frac{\Omega_2}{2}\varrho_{a2} + \left(i(\Delta_3 - \Delta_2) - \frac{\Gamma_b^0}{2} - \frac{1}{2}\Gamma_2\sum_{\mathbf{k}}\beta_{\mathbf{k}2}(N_{\mathbf{k}3} + 1)\right)\varrho_{b2}, \quad \text{(B8)}$$

$$\frac{d}{dt}\varrho_{a2} = i\frac{\Omega_1}{2}\rho_{12} + i\frac{\Omega_2}{2}\varrho_{b2} - i\frac{\Omega_3}{2}\varrho_{ba}^* + \left(i(\Delta_1 + \Delta_3) - \frac{1}{2}\Gamma_a^0 - \sum_{\mathbf{k}}\Gamma_2\beta_{\mathbf{k}2}(N_{\mathbf{k}3} + 1)\right)\varrho_{a2} \quad \text{(B9)}$$

$$\frac{d}{dt}\varrho_{21} = -i\frac{\Omega_1}{2}\rho_{a2}^* + i\frac{\Omega_3^*}{2}\varrho_{b1} + \left[i\Delta_3 - \frac{1}{2}\Gamma_1 - \sum_{\mathbf{k}}\left(\Gamma_2\beta_{\mathbf{k}2}(N_{\mathbf{k}3} + 1) - \alpha_{41}\Gamma_4^0\beta_{\mathbf{k}4}N_{\mathbf{k}4}\right)\right]\varrho_{21} \quad \text{(B10)}$$

$$\frac{d}{dt}N_{\mathbf{k}3} = \frac{i}{2}\left(\Omega_4\varrho_{\mathbf{k}43} - c.c\right) + \Gamma_2\beta_{\mathbf{k}2}N_2(N_{\mathbf{k}3} + 1) - \Gamma_3 N_3, \quad \text{(B11)}$$

$$\frac{d}{dt}N_{\mathbf{k}4} = -\frac{i}{2}\left(\Omega_4\varrho_{\mathbf{k}43} - c.c\right) - \Gamma_4^0 N_{\mathbf{k}4}(\alpha_{41}\beta_{\mathbf{k}4}N_1 + 1), \quad \text{(B12)}$$

$$\frac{d}{dt}\varrho_{\mathbf{k}43} = i\frac{\Omega_4}{2}(N_{\mathbf{k}3} - N_{\mathbf{k}4}) + \frac{1}{2}\left(\Gamma_2\mu_{\mathbf{k}2}N_2 - \Gamma_3 - \Gamma_4^0(\alpha_{41}\mu_{\mathbf{k}4}N_1 + 1)\right)\varrho_{\mathbf{k}43}, \quad \text{(B13)}$$

assuming all $\Omega's$ are real. Here, $\Delta_j$ $(j = 1, 2, 3)$ is the detuning indicated in figure 5 (a). $\Gamma_a^0$, $\Gamma_b^0$, $\Gamma_2$ and $\Gamma_4^0$ are the natural linewidths of states $|a\rangle$, $|b\rangle$, $|2\rangle$ and $|4\rangle$, respectively. $\alpha_{41}$ is the branch percentage for $|4\rangle$ to spontaneously decay to $|1\rangle$, so that $\Gamma_4 = \alpha_{41}\Gamma_4^0$ is the spontaneous decay rate from $|4\rangle$ to $|1\rangle$. $\Gamma_1 = \frac{\Omega_4^2}{4\Delta_3^2}\Gamma_a$ is the effective loss rate of $|1\rangle$ atoms, due to being excited by the detuned laser $\Omega_4$ to the unstable upper level $|a\rangle$. Similarly, $\Gamma_3 = \frac{\Omega_1^2}{4(\Delta_1 - \Delta_3)^2}\Gamma_4^0$ is the effective loss rate for atoms in $|3\rangle$, induced by laser $\Omega_1$. We note the above rate-equation model has only incorporated dominant atom loss mechanism for each atomic level.


[1] D. Bouwmeester, A. Ekert, and A. Zeilinger, *The Physics of Quantum information* (Springer-Verlag, Berlin, 2000).

[2] M. O. Scully and M. S. Zubairy, *Quantum Optics* (Cambridge University Press, NewYork, USA, 1997).

[3] S. Gröblacher, T. Paterek, R. Kaltenbaek, C. Brukner, M. Żukowski, M. Aspelmeyer, and A. Zeilinger, Nature **446**, 871 (2007).

[4] M. Greiner, O. Mandel, T. Esslinger, T. W. Hänsch, and I. Bloch, Nature (London) **415**, 39 (2002).

[5] D. Bouwmeester, J.-W. Pan, K. Mattle, M. Eibl, H. Weinfurter, and A. Zeilinger, Nature **390**, 575 (1997).

[6] A. Migdall, R. Datla, A. Sergienko, J. S. Orszak, and Y. H. Shih, Appl. Opt. **37**, 3455 (1998).

[7] M. D. Lukin, Rev. Mod. Phys. **75**, 457 (2003).

[8] M. Fleischhauer, A. Imamoglu, and J. P. Marangos, Reviews of Modern Physics **77**, 633 (2005).

[9] J. F. Sherson, H. Krauter, R. K. Olsson, B. Julsgaard, K. Hammerer, I. Cirac, and E. S. Polzik, Nature **443**, 557 (2006).

[10] V. Boyer, M. A. Marino, R. C. Pooser, and P. D. Lett, Science **321**, 544 (2008).

[11] H. J. Kimble, Nature **453**, 1023 (2008).

[12] S. E. Harris, M. K. Oshman, and R. L. Byer, Phys. Rev. Lett. **18**, 732 (1967).

[13] F. König, E. J. Mason, F. N. C. Wong, and M. A. Albota, Phys. Rev. A **71**, 033805 (2005).

[14] A. S. Zibrov, M. D. Lukin, and M. O. Scully, Phys. Rev. Lett. **83**, 4049 (1999).

[15] C. H. van der Wal, M. D. Eisamen, A. Andre, R. L. Walsworth, D. F. Phillips, A. S. Zibrov, and M. D. Lukin, Science **301**, 196 (2003).

[16] A. Kuzmich, W. P. Bowen, A. D. Boozer, A. Boca, C. W. Chou, L. M. Duan, and H. J. Kimble, Nature **423**, 731 (2003).

[17] V. Balić, D. A. Braje, P. Kolchin, G. Y. Yin, and S. E. Harris, Phys. Rev. Lett. **94**, 183601 (2005).

[18] P. Kolchin, S. Du, C. Belthangady, G. Y. Yin, and S. E. Harris, Phys. Rev. Lett. **97**, 113602 (2006).

[19] J. Thompson, J. Simon, H. Loh, and V. Vuletic, Science **313**, 74 (2006).

[20] T. Chanelière, D. N. Matsukevich, S. D. Jenkins, T. A. B. Kennedy, M. S. Chapman, and A. Kuzmich, Phys. Rev. Lett. **96**, 093604 (2006).

[21] S. Du, J. Wen, M. H. Rubin, and G. Y. Yin, Phys. Rev.

Lett. **98**, 053601 (2007).
[22] S. Du, P. Kolchin, C. Belthangady, G. Y. Yin, and S. E. Harris, Phys. Rev. Lett. **100**, 183603 (2008).
[23] R. H. Dicke, Phys. Rev. **93**, 99 (1954).
[24] E. Paradis, B. Barrett, K. A., R. Zhang, and G. Raithel, Phys. Rev.A **77**, 043419 (2008).
[25] L. M. Duan, M. D. Lukin, J. I. Cirac, and P. Zoller, Nature **414**, 413 (2001).
[26] A. Aspect, G. Roger, S. Reynaud, J. Dalibard, and C. Cohen-Tannoudji, Phys. Rev. Lett. **45**, 617 (1980).
[27] P. Grangier, G. Roger, A. Aspect, A. Heidmann, and S. Reynaud, Phys. Rev. Lett. **57**, 687 (1986).
[28] C. H. R. Ooi and M. O. Scully, Phys. Rev. A **76**, 043822 (2007).
[29] M. G. Moore and P. Meystre, Phys. Rev. Lett. **83**, 5202 (1999).
[30] M. Lax, Phys. Rev. **172**, 350 (1968).
[31] F. T. Arecchi and E. Courtens, Phys. Rev. A **2**, 1730 (1970).
[32] R. Bonifacio, P. Schwendimann, and F. Haake, Phys. Rev. A **4**, 302 (1971).
[33] M. M. Salour, Rev. Mod. Phys. **50**, 667 (1978).
[34] J. Stenger, S. Inouye, A. P. Chikkatur, D. M. Stamper-Kurn, D. E. Pritchard, and W. Ketterle, Phys. Rev. Lett. **82**, 4569 (1999).
[35] M. G. Moore, O. Zobay, and P. Meystre, Phys. Rev. A **60**, 1491 (1999).
[36] B. Yurke, S. L. McCall, and J. R. Klauder, Phys. Rev. A **33**, 4033 (1986).
[37] M. J. Holland and K. Burnett, Phys. Rev. Lett. **71**, 1355 (1993).
[38] Y. P. Huang and M. G. Moore, Phys. Rev. A **77**, 032349 (2008).
[39] S. E. Harris, J. E. Field, and A. Imamoğlu, Phys. Rev. Lett. **64**, 1107 (1990).